Cellular and Molecular Life Sciences (2023) 80:91
https://doi.org/10.1007/s00018-023-04752-5

ORIGINAL ARTICLE

KIF13B mediates VEGFR2 recycling to modulate vascular permeability

Hyun-Dong Cho[1,3] · Nguyễn Thị Thanh Nhàn[1] · Christopher Zhou[1] · Kayeman Tu[1] · Tara Nguyen[2] · Nicolene A. Sarich[1] · Kaori H. Yamada[1,2]

Received: 6 July 2022 / Revised: 4 March 2023 / Accepted: 6 March 2023 / Published online: 16 March 2023

Abstract

Excessive vascular endothelial growth factor-A (VEGF-A) signaling induces vascular leakage and angiogenesis in diseases. VEGFR2 trafficking to the cell surface, mediated by kinesin-3 family protein KIF13B, is essential to respond to VEGF-A when inducing angiogenesis. However, the precise mechanism of how KIF13B regulates VEGF-induced signaling and its effects on endothelial permeability is largely unknown. Here we show that KIF13B-mediated recycling of internalized VEGFR2 through Rab11-positive recycling vesicle regulates endothelial permeability. Phosphorylated VEGFR2 at the cell–cell junction was internalized and associated with KIF13B in Rab5-positive early endosomes. KIF13B mediated VEGFR2 recycling through Rab11-positive recycling vesicle. Inhibition of the function of KIF13B attenuated phosphorylation of VEGFR2 at Y951, SRC at Y416, and VE-cadherin at Y685, which are necessary for endothelial permeability. Failure of VEGFR2 trafficking to the cell surface induced accumulation and degradation of VEGFR2 in lysosomes. Furthermore, in the animal model of the blinding eye disease wet age-related macular degeneration (AMD), inhibition of KIF13B-mediated VEGFR2 trafficking also mitigated vascular leakage. Thus, the present results identify the fundamental role of VEGFR2 recycling to the cell surface in mediating vascular permeability, which suggests a promising strategy for mitigating vascular leakage associated with inflammatory diseases.

Keywords VEGFR2 · Endothelial permeability · Kinesin · Trafficking · Vesicle · Eye diseases

Introduction

Leakage from blood vessels at the level of endothelial cell junctions causes tissue inflammation in many diseases, including cancer and blinding eye diseases [2]. Endothelial cells lining the vessel wall have adherens junctions and tight junctions, which serve as barriers limiting the permeation of molecules and liquid [2, 3]. In diseased conditions, excessive vascular endothelial growth factor-A (VEGF-A) induces unchecked angiogenesis and vascular leakage [2, 4, 5]. We have developed a new strategy to inhibit pathological angiogenesis in cancer [6] and wet age-related macular degeneration (wet AMD) [7], the leading cause of blindness. However, it remains unknown whether this approach also prevents endothelial permeability and the mechanism. Here we show that inhibition of VEGFR2 trafficking to the plasma membrane was critical in controlling endothelial permeability.

The cell surface receptor for VEGF-A, VEGFR2, is trafficked between the cell surface and intra-endothelial domains [8]. VEGFR2 in the quiescent endothelium is normally present in a dephosphorylated inactive state on the endothelial cell surface [8]. Upon binding to VEGF-A, phosphorylation of VEGFR2 rapidly induces internalization [9, 10] and trafficking into early endosomes and its colocalization with Rab5 [11]. VEGFR2 is subsequently dephosphorylated [12] before entering Rab11 recycling vesicles [13]. Part of the VEGFR2 pool is sorted for recycling to the cell surface [8] to make the receptor available for another round of ligand binding [11, 14, 15]. The non-cycled part of VEGFR2 undergoes degradation through Rab7-positive late endosomes and lysosomal

✉ Kaori H. Yamada
horiguch@uic.edu

1 Department of Pharmacology and Regenerative Medicine, University of Illinois College of Medicine, Chicago, IL 60612, USA

2 Department of Ophthalmology and Visual Sciences, University of Illinois College of Medicine, Chicago, IL 60612, USA

3 Present Address: Department of Food and Nutrition, Sunchon National University, Sunchon 57922, Republic of Korea

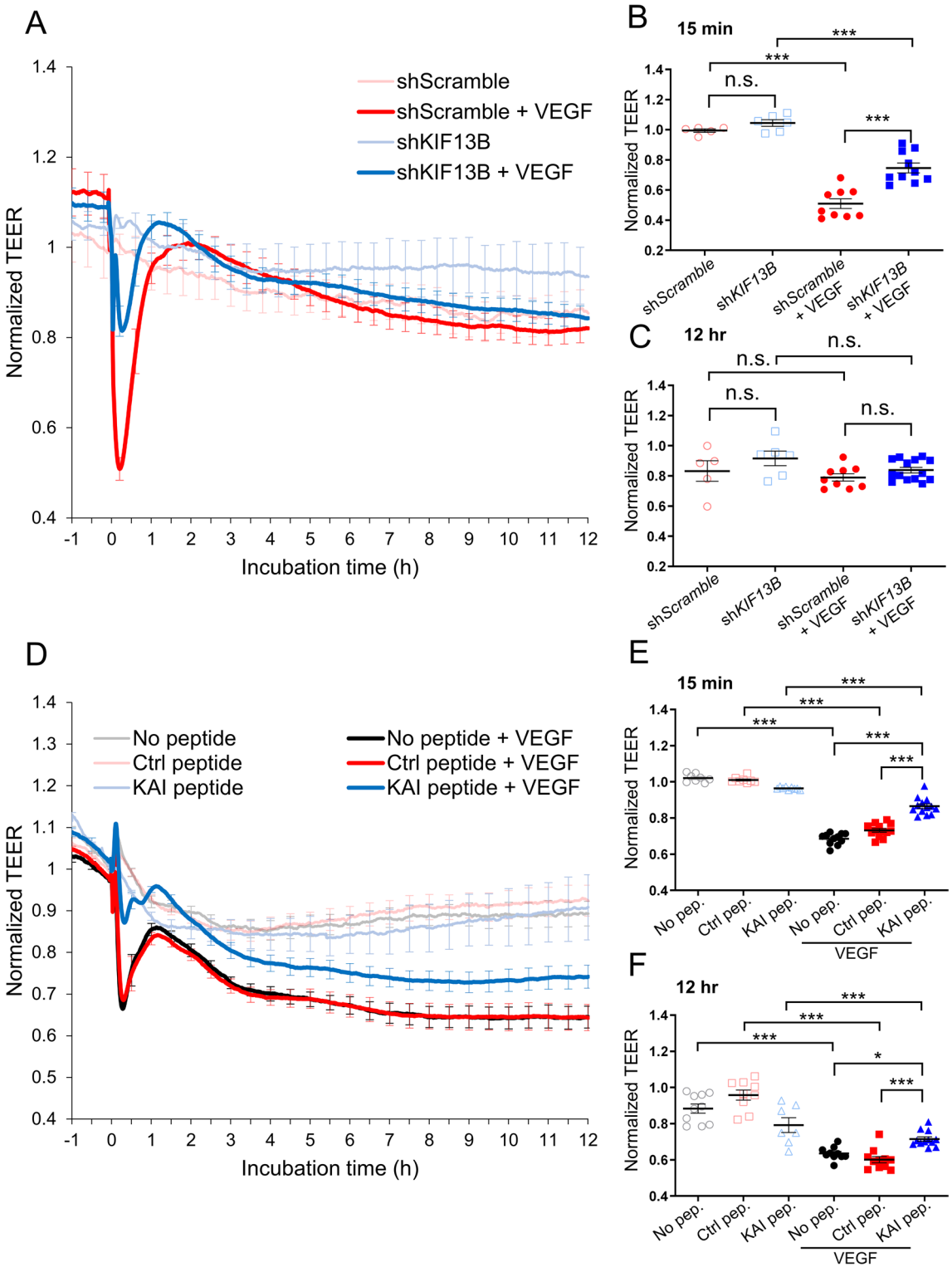

membrane-associated protein 2 (LAMP2)-positive lysosome [8]. To restore VEGFR2 levels on the plasmalemma, newly synthesized VEGFR2 is trafficked from the Golgi apparatus to the cell surface [14, 16]. We found that trafficking of VEGFR2 from the Golgi apparatus to the cell surface is mediated by a kinesin-3 family molecular motor KIF13B [16]. KIF13B knockout mice (*Kif13b*^{KO}) showed reduced angiogenesis [7]. Endothelial-specific inducible KIF13B knockout (*Kif13b*^{iECKO}) also showed reduced angiogenesis, vascular leakage, and cancer metastasis [17]. Furthermore, the pharmacological

◂**Fig. 1** KIF13B is essential for VEGF-induced permeability in hREC. **A**, **B**, **C** Transendothelial electrical resistance (TEER) measurement of confluent hRECs transduced with scrambled shRNA (red and pink lines) or shRNA-*KIF13B* (blue and light blue) expressed as normalized resistance of the TEER basal values. Cells were stimulated with VEGF-A (50 ng/mL) at time zero, and TEER was measured every 30 s over time (4000 Hz of frequency). Normalized resistance changes overtime were shown in graph **A**. Normalized resistance at 15 min after VEGF-A stimulation and 12 h after VEGF-A stimulation were shown in **B**, and **C** as mean ± SE. N = 5, 6, 18, 18, for scrambled shRNA, shRNA-*KIF13B*, scrambled shRNA + VEGF-A, and shRNA-*KIF13B* + VEGF-A, respectively. The graphs in **B** and **C** show N = 5, 6, 9, 10 and N = 5, 6, 9, 14, respectively, by excluding outliners of mean ± 4 × SE. Note, including outliners and excluding outliners did not affect statistical analyses. One-way ANOVA with post hoc multiple comparisons. ***$p < 0.001$. **D–F** TEER measurements of hREC treated with KAI (10 µM), an inhibitor for VEGFR2 trafficking, or control peptide (10 µM) followed by VEGF-A (50 ng/mL) stimulation. Changes of normalized resistance over time were shown in graph **D**. Normalized resistance at 15 min and 12 h after VEGF-A stimulation were shown in E and F as mean ± SE. N = 12, 10, 13, 8, 16, 15, for no peptide, ctrl, KAI, no peptide + VEGF-A, ctrl + VEGF-A, KAI + VEGF-A, respectively. The graphs in **E** and **F** show N = 10, 9, 7, 10, 11, 12 and N = 8, 8, 9, 11, 13, 13, respectively, by excluding outliners of mean ± 4 × SE. Note, including outliners and excluding outliners did not affect statistical analyses. One-way ANOVA with post hoc multiple comparisons. *$p < 0.05$, **$p < 0.01$

disruption of the interaction between KIF13B and VEGFR2 inhibited vascular leakage [17] and neovascularization [7].

Although VEGF-A induces angiogenesis and endothelial permeability, the signaling pathways are different [2, 8]. Phosphorylation of VEGFR2 at Y951 recruits T cell-specific adaptor (TSAd), which regulates activation of c-SRC tyrosine kinase [18]. SRC-mediated phosphorylation of Y685 of VE-cadherin is essential to increase endothelial permeability by VEGF-A [19–21]. Although the importance of VEGFR2 trafficking for angiogenesis is well known, we surmised whether VEGFR2 trafficking might also regulate endothelial permeability, relatively rapid response occurring within minutes [2] as contrasted with angiogenesis requiring hours [8]. Here we addressed mechanisms regulating VEGF-A-induced endothelial permeability. Among the approaches employed was the peptide KAI (kinesin-derived angiogenesis inhibitor), which inhibits KIF13B-mediated VEGFR2 trafficking [6] as well as knockdown of the molecular motor KIF13B in endothelial cells that traffics the receptor to the plasma membrane. We showed the crucial role of KIF13B mediated VEGFR2 trafficking to plasma membrane in regulating VEGF-A endothelial permeability.

Results

KIF13B regulates VEGF-induced endothelial permeability

KIF13B transports newly synthesized VEGFR2 from Golgi to the cell surface [16], and the VEGFR2 trafficking is essential for angiogenesis [6, 7, 16]. We showed that KIF13B also plays an important role in VEGF-induced vascular leakage, as VEGF-A fails to induce vascular leakage in $Kif13b^{ECKO}$ or when KIF13B-mediated VEGFR2 trafficking is blocked by KAI [17]. However, VEGF-induced endothelial permeability is an early response of ECs to VEGF-A, occurring within 15 min. It cannot be explained by the known function of KIF13B, which is the release of synthesized VEGFR2 from Golgi and its trafficking to the cell surface, taking several hours after VEGF-A stimulation [16]. To explore whether KIF13B has any role in the relatively rapid response to VEGF-A, we used lentivirus-based shRNA-*KIF13B* to knockdown (Supplemental Fig. S1A, B) [16], and tested VEGF-induced endothelial permeability in human retina endothelial cells (hREC) using transendothelial electric resistance (TEER) assay. VEGF-A transiently reduced TEER at 15 min after VEGF-A stimulation in control hREC, transduced with scrambled shRNA (Fig. 1A, B), whereas knockdown of *KIF13B* suppressed VEGF-induced endothelial permeability compared to controls (Fig. 1A, B). After initial permeability, the endothelial barrier function recovered in both scrambled and shRNA-*KIF13B* treated cells (Fig. 1A, C).

Next, we tested whether the inhibition of VEGFR2 trafficking also affects endothelial permeability (Fig. 1D–F). KAI is a synthetic peptide designed to disrupt the interaction between VEGFR2 and KIF13B [6]. We confirmed the effect of KAI on the interaction between KIF13B and VEGFR2 by co-immunoprecipitation (co-IP). Consistent with a previous report [16], VEGF induced the interaction between KIF13B and VEGFR2 in control cells, whereas KAI prevented their interaction (Supplemental Fig. S1C, D). After pretreatment with the control peptide (scrambled KAI) or KAI (10 µM) for 2 h, hRECs were stimulated with VEGF-A. The TEER of confluent hREC was monitored before and after VEGF-A stimulation (Fig. 1D). KAI treatment prevented VEGF-induced endothelial permeability, compared to no-peptide control and control peptide-treated hREC (Fig. 1D). KAI-treated hREC showed higher electrical resistance values than both no peptide and control peptide-treated cells 15 min and 12 h after stimulation with VEGF-A (Fig. 1D–F). This data demonstrates that KIF13B is required for VEGF-induced endothelial permeability.

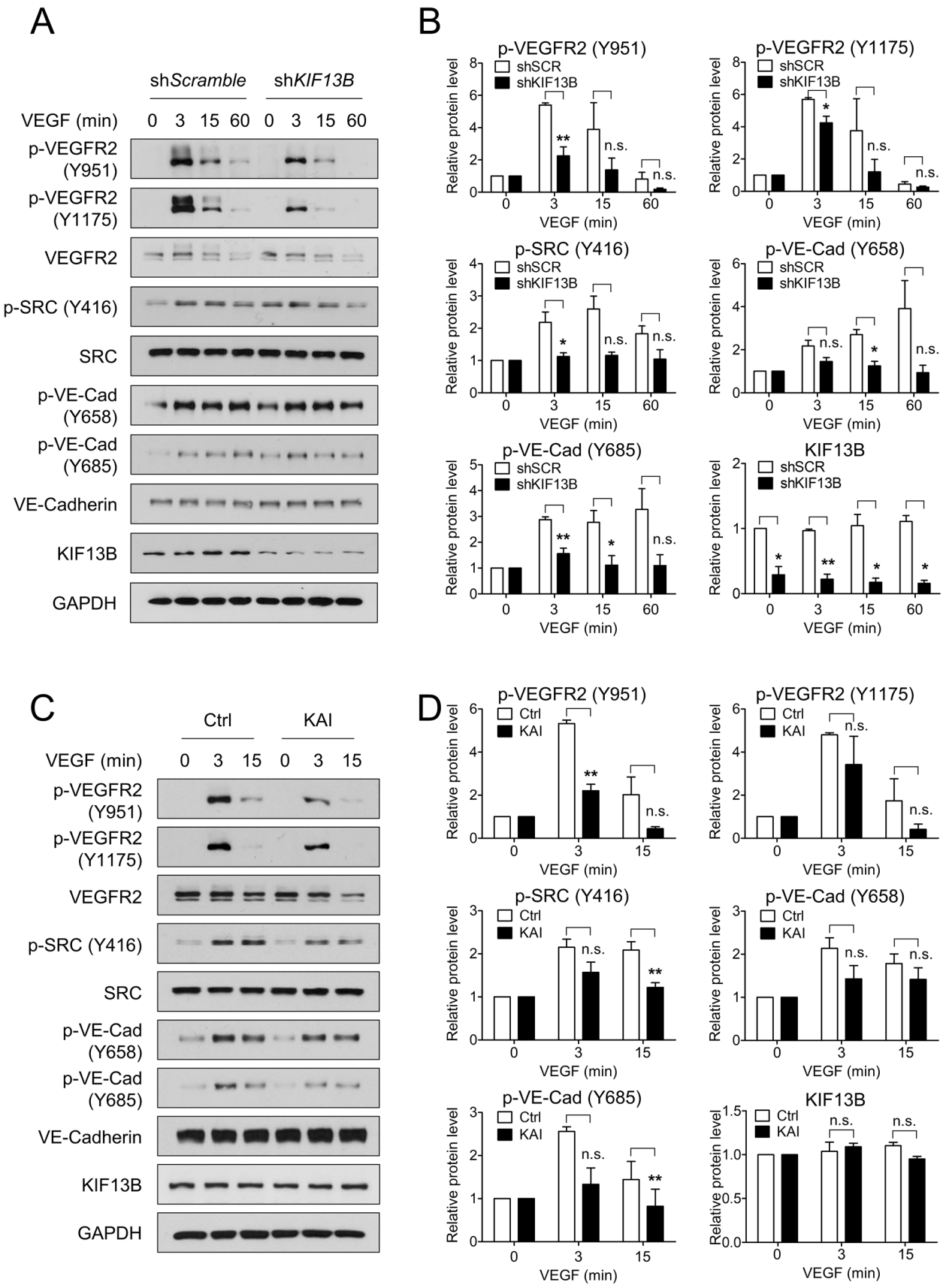
A
shScramble
shKIF13B
VEGF (min) 0 3 15 60 0 3 15 60
p-VEGFR2 (Y951)
p-VEGFR2 (Y1175)
VEGFR2
p-SRC (Y416)
SRC
p-VE-Cad (Y658)
p-VE-Cad (Y685)
VE-Cadherin
KIF13B
GAPDH
B
p-VEGFR2 (Y951)
p-VEGFR2 (Y1175)
p-SRC (Y416)
p-VE-Cad (Y658)
p-VE-Cad (Y685)
KIF13B
shSCR
shKIF13B
Relative protein level
VEGF (min)
n.s.
C
Ctrl
KAI
VEGF (min) 0 3 15 0 3 15
p-VEGFR2 (Y951)
p-VEGFR2 (Y1175)
VEGFR2
p-SRC (Y416)
SRC
p-VE-Cad (Y658)
p-VE-Cad (Y685)
VE-Cadherin
KIF13B
GAPDH
D
p-VEGFR2 (Y951)
p-VEGFR2 (Y1175)
p-SRC (Y416)
p-VE-Cad (Y658)
p-VE-Cad (Y685)
KIF13B
Ctrl
KAI
Relative protein level
VEGF (min)
n.s.

◂**Fig. 2** KIF13B is required to regulate VEGFR2 signaling pathway. **A**, **B** VEGF-induced phosphorylation of signaling molecules in hREC transduced with either scrambled shRNA or shRNA-*KIF13B*. After stimulation with VEGF-A (50 ng/mL) for indicated time points, cell lysates were analyzed by western blotting for p-VEGFR2 (Y951), p-VEGFR2 (Y1175), VEGFR2, p-SRC (Y416), SRC, p-VE-cadherin (Y658), p-VE-cadherin (Y685), VE-cadherin, KIF13B, and GAPDH (p indicates the phosphorylated form). Representative blots were shown in **A**. Quantification of blots of phosphorylated proteins expressed relative to total proteins were shown as mean ± SE in graph **B**. N = 3. One-way ANOVA followed by post hoc multiple comparisons. $*p < 0.05$, $**p < 0.01$. No significant difference (n.s.) indicates $p > 0.05$. **C**, **D** VEGF-induced phosphorylation of signaling molecules in hREC treated with either control peptide or KAI (10 μM). After stimulation with VEGF-A (50 ng/mL) for indicated time points, cell lysates were analyzed by western blotting for phosphorylated and total proteins. Representative blots were shown in **C**. Quantification of phosphorylated proteins relative to total proteins was shown as mean ± SE in graph **D**. N = 4. One-way ANOVA followed by post hoc multiple comparisons. $**p < 0.01$. n.s. indicates $p > 0.05$

KIF13B regulates VEGFR2 signaling pathways mediating endothelial permeability

To examine how KIF13B regulates endothelial permeability, we examined the activation of the signaling pathway regulating endothelial permeability and tested the effect of knockdown of *KIF13B* (Fig. 2A, B). VEGF-A treatment increased phosphorylation of VEGFR2 (at Y951 and Y1175), SRC (at Y416), and VE-cadherin (at Y658 and Y685) in scrambled shRNA transduced control hREC. Compared to scrambled shRNA transduced cells, shRNA-*KIF13B* transduced cells showed significantly lower phosphorylated/total protein ratio in p-VEGFR2 (Y951 and Y1175), p-SRC (Y416), and p-VE-cadherin (Y658 and Y685) through 3–15 min of VEGF-A treatment (Fig. 2A, B). Although knockdown of *KIF13B* increased basal phosphorylation of SRC, stimulation with VEGF further increased phosphorylation of SRC in both control and KIF13B knockdown cells (Fig. 2A, Supplemental Fig. S2A). Knockdown of *KIF13B* prevented VEGF-induced phosphorylation of SRC to some extent in all time points (Fig. 2B, Supplemental Fig. S2A).

Next, we tested the effect of KAI compared with the control peptide (Fig. 2C, D). Similar to scrambled shRNA treated control above, VEGF-A induced p-VEGFR2 (at Y951 and Y1175), p-SRC (at Y416), and p-VE-cadherin (at Y658 and Y685) in control peptide-treated hREC (Fig. 2C, D). KAI treatment significantly decreased phosphorylation of VEGFR2 (Y951), SRC (Y416), and VE-cadherin (Y685) compared with control peptide treatment (Fig. 2C, D). KAI treatment also decreased p-VEGFR2 (Y1175) and pY658-VE-cadherin, although the difference was not statistically significant. Then, we tested the effect of KAI on another phosphorylation site of VEGFR2, Y1059. VEGF-induced autophosphorylation on Y1059 indicates dimerization and kinase activity of VEGFR2 [8]. Pretreatment with KAI did not affect the initial phosphorylation of VEGFR2 at Y1059 at 3 min after VEGF stimulation (Supplemental Figure S2B, C), indicating proper dimerization and activation of its kinase activity of VEGFR2. At 15 min after VEGF stimulation, p-VEGFR2 at Y1059 was decreased in KAI-treated cells compared to control, suggesting faster dephosphorylation/inactivation. Together, this data suggests the important role of KIF13B in regulating VEGF/VEGFR2 signaling to regulate endothelial permeability.

KIF13B regulates translocation of internalized VEGFR2

As KIF13B mediates VEGFR2 trafficking to the cell surface [16], we hypothesized that KIF13B tunes the degree of VEGF/VEGFR2 signaling by regulating the amount of VEGFR2 on the cell surface. We examined the effect of the knockdown of *KIF13B* on cell surface VEGFR2 before and after VEGF-A stimulation (Fig. 3). First, hREC were transduced with scrambled shRNA or shRNA-*KIF13B*, and stimulated with VEGF-A for indicated times. Cell surface proteins were biotinylated and precipitated with streptavidin beads, and biotinylated cell surface VEGFR2 was detected by western blotting (Fig. 3A, B). Cell surface VEGFR2 was decreased at 15–30 min after VEGF-A stimulation in both control and shRNA-*KIF13B* transduced hRECs, indicating VEGF-induced internalization (Fig. 3A, B). Interestingly, the knockdown of *KIF13B* further decreased the amount of VEGFR2 on the cell surface (Fig. 3B).

We further examined the effect of KAI on cell surface VEGFR2 by immunostaining with the antibody against the extracellular domains of VEGFR2 (Fig. 3C, D). Cells were mildly fixed to avoid cell membrane permeability as described [16], and stained with antibodies against VEGFR2 and VE-cadherin. The intensity of cell surface VEGFR2 was gradually decreased after VEGF stimulation in both control peptide-treated cells and KAI-treated cells. KAI treatment accelerated the decrease of cell surface VEGFR2 at 30 min after VEGF stimulation (Fig. 3C, D), showing a similar observation seen by knockdown of *KIF13B* (Fig. 3A, B).

As a portion of internalized VEGFR2 is recycled back to the cell surface [8], the reduction of cell-surface VEGFR2 may be the result of increased internalization or less recycling. Thus, we used another biotinylation assay [22] to quantify internalized VEGFR2 (Fig. 3E–G). hRECs were transduced with scrambled shRNA or shRNA-*KIF13B*. After the serum starvation of cells, cell surface proteins were biotinylated. Then, cells were stimulated with VEGF-A to let VEGFR2 internalize. After removal of cell surface biotin, internalized VEGFR2 was detected by western blotting in streptavidin precipitates (Fig. 3E–G). After VEGF-A stimulation, VEGFR2 was internalized in both control and shRNA-*KIF13B* transduced cells without any difference

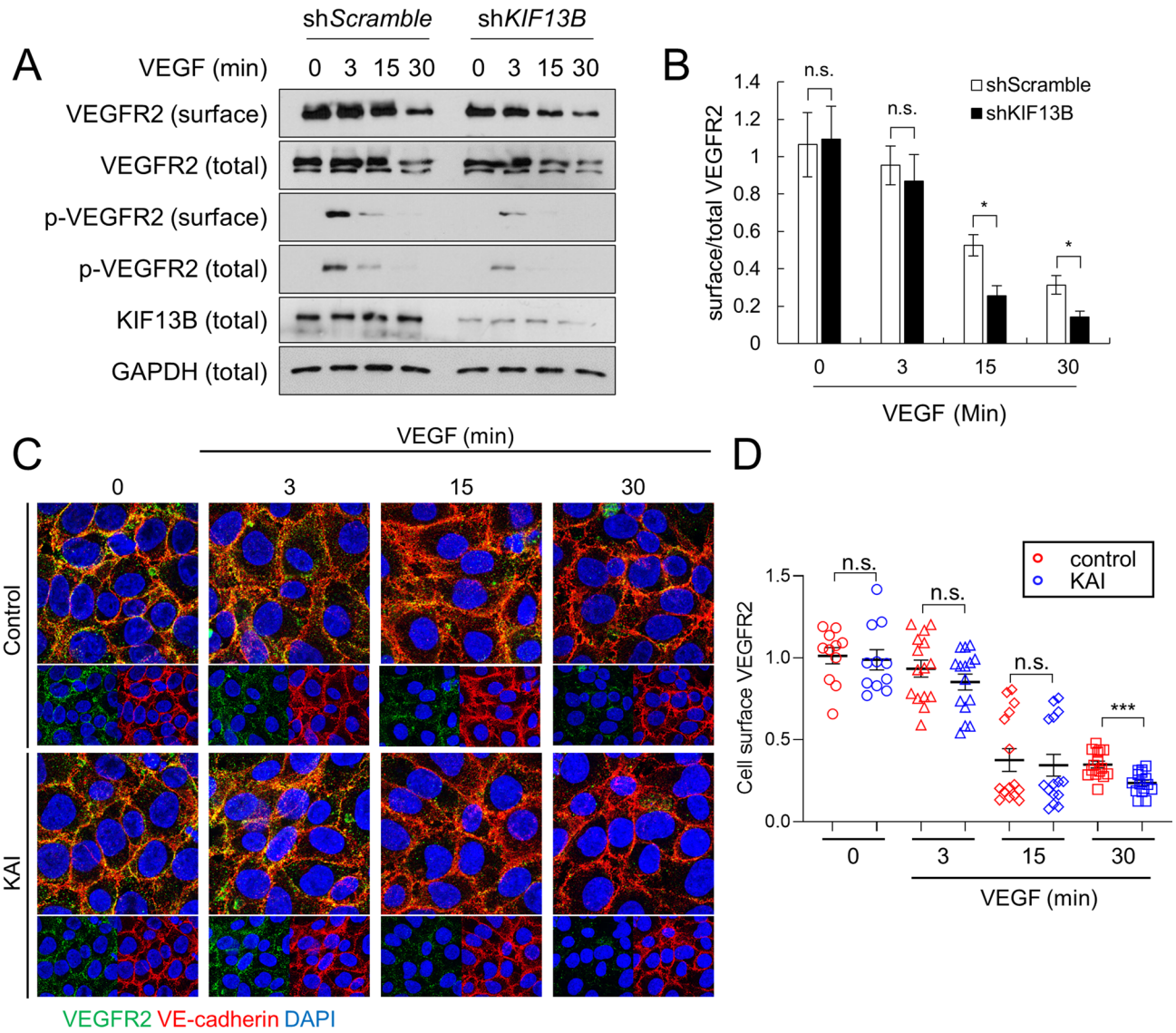
A
shScramble
shKIF13B
VEGF (min)
0 3 15 30 0 3 15 30
VEGFR2 (surface)
VEGFR2 (total)
p-VEGFR2 (surface)
p-VEGFR2 (total)
KIF13B (total)
GAPDH (total)
B
shScramble
shKIF13B
surface/total VEGFR2
n.s.
n.s.
*
*
VEGF (Min)
C
VEGF (min)
0
3
15
30
Control
KAI
VEGFR2 VE-cadherin DAPI
D
control
KAI
Cell surface VEGFR2
n.s.
n.s.
n.s.
***
VEGF (min)
E
shScramble
shKIF13B
VEGF (min)
0 3 15 30 0 3 15 30
VEGFR2 (Internalized)
VEGFR2 (total)
KIF13B (total)
GAPDH
F
shSCR
shKIF13B
Internalized/total VEGFR2
VEGF (min)
G
shSCR
shKIF13B
Internalized VEGFR2 / GAPDH
VEGF (min)

◂**Fig. 3** KIF13B deficiency reduces cell-surface VEGFR2 after VEGF stimulation. **A**, **B** Cell surface VEGFR2 levels detected by cell surface biotinylation of hREC transduced with either scrambled shRNA or shRNA-*KIF13B*, followed by VEGF-A stimulation (50 ng/mL) for indicated time periods. Total lysates (total) and streptavidin pull-down (surface), western blotting for VEGFR, p-VEGFR2 (Y1175) were shown in **A**. GAPDH was used as a loading control. Quantification of cell surface VEGFR2 was normalized by total VEGFR2, and shown as mean ± SE in graph **B**. N = 4. One-way ANOVA followed by multiple comparisons. *$p < 0.05$. n.s. indicates $p > 0.05$. **C**, **D** Immunostaining of cell surface VEGFR2 (green) and VE-cadherin (red) in hREC pretreated with control peptide or KAI peptide followed by VEGF stimulation for indicated times. Goat antibody for extracellular domain of VEGFR2 and mouse antibody for extracellular domain of VE-cadherin were used for staining of cells without detergent-permeabilization. Intensity of VEGFR2 was quantified by Image J and shown as mean ± SE in the graph. N = 11, 11, 15, 15, 15, 15, 15, 15 for control 0 min, KAI 0 min, control 3 min, KAI 3 min, control 15 min, KAI 15 min, control 30 min, KAI 30 min, respectively. N is number of pictures analyzed from 3 independent experiments. Student's t test. *$p < 0.05$. **E–G** The internalized pool of VEGFR2 after VEGF-A treatment (50 ng/mL) of hREC transduced with either scrambled shRNA or shRNA-*KIF13B*. Cell surface biotinylation was performed prior to VEGF-A stimulation. At indicated time points, the remaining cell surface biotin was removed, and the internalized pool of VEGFR2 was collected by streptavidin pull-down. Western blotting of the total lysate (total) and streptavidin pull-down (internalized) for VEGFR2 was shown in **E**. Internalized VEGFR2 was normalized by total VEGFR2 or loading control GAPDH, and shown as mean ± SE in the graph **F** and **G**, respectively. N = 3. One-way ANOVA followed by multiple comparisons and Student's t test did not find any statistical significance between sh*Scr* and sh*KIF13B*

(Fig. 3E–G), suggesting the possibility of KIF13B mediating recycling of internalized VEGFR2.

To further examine the question of localization of VEGFR2 and p-VEGFR2, we stained hRECs with their respective antibodies (Supplemental Fig. S3). Before VEGF-A stimulation, the majority of VEGFR2 localized near nuclei as in [14, 16]. And a portion of VEGFR2 was also observed at cell–cell junctions in both control peptide-treated and KAI-treated cells (Supplemental Fig. S3). Three min after VEGF-A stimulation, phosphorylation of VEGFR2 (Y1175) was mainly observed at cell–cell junctions (Supplemental Fig. S3). To confirm the localization of p-VEGFR2 (Y1175) at the cell–cell junctions, we also stained the confluent cells with the antibodies against p-VEGFR2 (Y1175) and VE-cadherin (Fig. 4A). Phosphorylation of VEGFR2 at cell–cell junctions, co-localized with VE-cadherin, was observed in both control-peptide treated cells and KAI-treated cells 3 min after VEGF stimulation (Fig. 4A, B). In control peptide-treated hREC, p-VEGFR2 was rapidly internalized and distributed in the cells 15 min after VEGF-A stimulation (Fig. 4A, Supplemental Fig. S3). However, p-VEGFR2 accumulated in KAI-treated hREC 15 min and 30 min after VEGF-A stimulation. The number of cells showing p-VEGFR2 accumulation was significantly increased in KAI-treated cells 15 min and 30 min after VEGF-A stimulation (Fig. 4D). The fluorescence intensity of p-VEGFR2 was not different between the two groups 3 min after VEGF stimulation, and decreased in KAI-treated cells 15 min after VEGF stimulation (Fig. 4C). Although the amount of p-VEGFR2 was reduced in KAI-treated hREC at 15 min, it strongly accumulated as vesicles-like in KAI-treated hREC, whereas p-VEGFR2 was distributed throughout in the control cells. Thus, the question arises about the disposition of VEGFR2 during the inhibition of VEGFR2 trafficking.

Inhibition of VEGFR2 recycling localizes VEGFR2 in late endosomes

Rab family GTPases localize to specific intracellular compartments where they regulate cargo trafficking [23]. Internalized VEGFR2 localizes at Rab5 positive early endosome, then post-dephosphorylation, VEGFR2 enters either Rab11-mediated recycling pathway or Rab7-mediated degradation pathway. To determine how KIF13B contributes to VEGFR2 trafficking, we performed co-IP with Rab family proteins, Rab5, Rab11, and Rab7, and analyzed binding proteins by western blotting (Fig. 5). Co-IP with Rab5, Rab7, and Rab11 could separate each endosomal compartment, as endosomal markers for early endosome (EEA1), late endosome (LAMP2), and recycling endosome (EXOC6) were selectively detected in co-IP with Rab5, Rab7, and Rab11, respectively (Supplemental Fig. S4). In control peptide-treated control hREC, VEGFR2 and KIF13B were co-immunoprecipitated with Rab5 (Fig. 5A). KAI treatment decreased KIF13B in co-IP with Rab5, whereas VEGFR2 remained co-precipitated with Rab5 (Fig. 5A, B). KAI treatment reduced VEGFR2 associated with Rab11, recycling endosome marker (Fig. 5C, D), suggesting reduced recycling in KAI-treated cells. The result was consistent with the biotinylation assay (Fig. 3) and showed the crucial role of KIF13B in mediating recycling of internalized VEGFR2. Upon inhibition of VEGFR2 trafficking by KAI treatment, we observed accumulation of p-VEGFR2 near nuclei (Fig. 4A). Inhibition of VEGFR2 recycling may thus traffic it to the degradation pathway.

To address this concept, we performed co-IP with a late endosome marker, Rab7 (Fig. 5E, F). In control hREC, p-VEGFR2 (Y1175) was detected in co-IP with Rab7 3 min after VEGF-A stimulation and dephosphorylated at 15 min (Fig. 5E). Interestingly, in KAI-treated hREC, accumulation of p-VEGFR2 was observed 3–15 min after VEGF stimulation in co-IP with Rab7, late endosome marker (Fig. 5E).

To confirm the western blotting results, we stained hREC with Rab11 and VEGFR2 (Supplemental Fig. S5A, B). In control peptide-treated cells, colocalization of VEGFR2 with recycling vesicle marker Rab11 was observed, but KAI treatment seemed to reduce colocalization 3 min and 15 min after

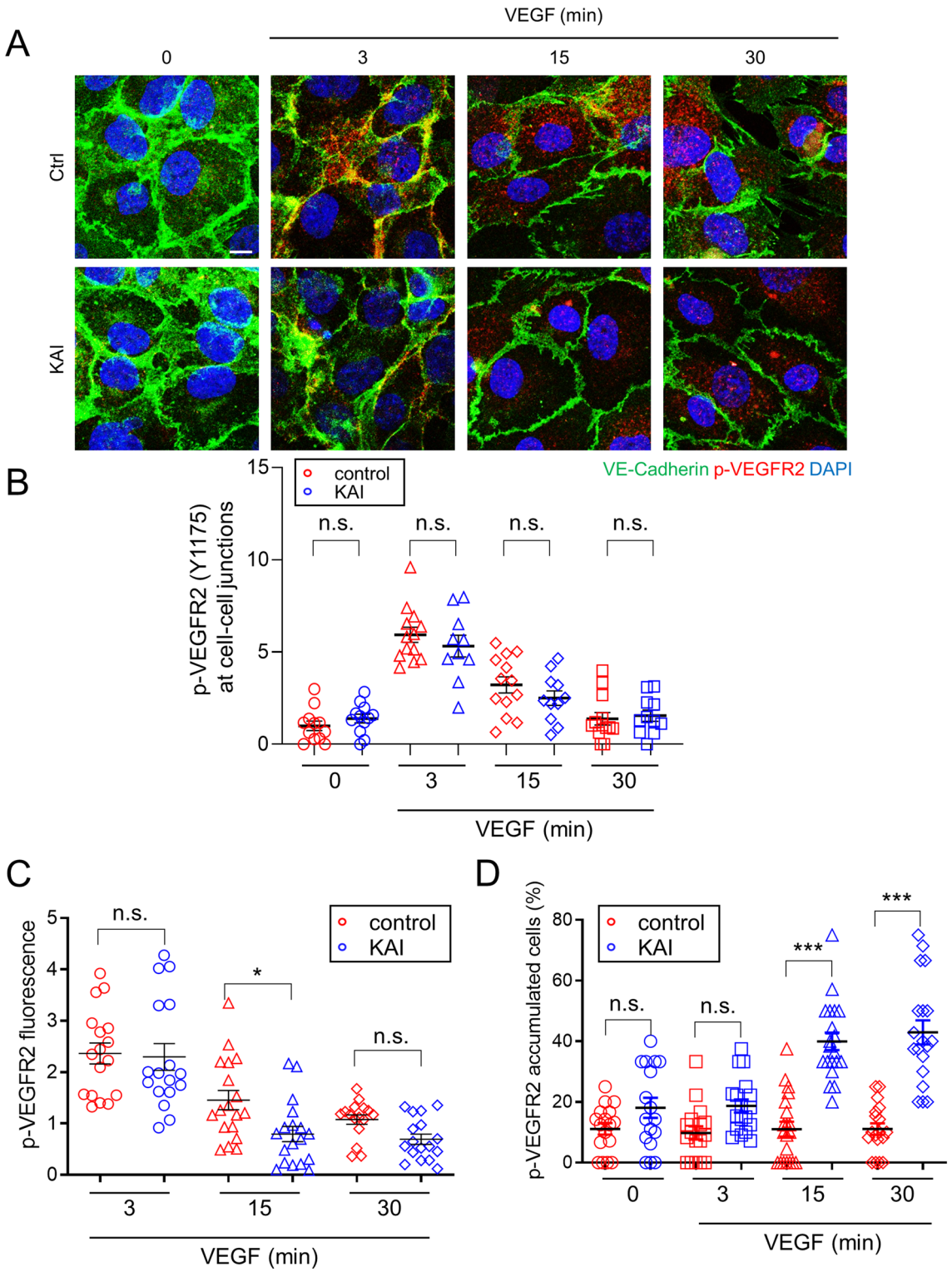

VEGF-A stimulation (Supplemental Fig. S5A, B). However, the immunostaining of endogenous Rab11 was like a cloud of vesicles throughout the cytoplasm, which prevented accurate quantification of the colocalization. To overcome the issue, we expressed Rab11-mCerulean at a low level in hREC (Supplemental Fig. S5C, Fig. 6), stained the cells with KIF13B and VEGFR2 to analyze their co-localization (Fig. 6). In control peptide-treated cells, colocalization of KIF13B and VEGFR2 was increased after VEGF stimulation (Fig. 6B), consistent with previous observation of

◂**Fig. 4** KIF13B regulates endosomal trafficking of phosphorylated VEGFR2. **A**, **B** Immunostaining for p-VEGFR2 (Y1175, red) and VE-cadherin (green) in hREC pretreated with either control peptide or KAI (10 μM) and stimulated with VEGF-A (50 ng/mL) for indicated time periods. Scale bars; 10 μm. The intensity of p-VEGFR2 at cell–cell junction (colocalized with VE-cadherin) was quantified by Image J and shown as mean ± SE in graph B. N = 13, 14, 14, 14, 13, 11, 13, 12 for pictures (from 3 independent experiments) in ctrl (0, 3, 15, 30 min), KAI (0, 3, 15, 30 min), respectively. Unpaired t test, n.s. indicates $p > 0.05$. **C** The intensity of p-VEGFR2 was quantified by Image J and shown as mean ± SE in graph C. N = 17, 18, 16, 17, 18, 17 (from 3 independent experiments) for pictures in ctrl (3, 15, 30 min), KAI (3, 15, 30 min). One-way ANOVA with post hoc multiple comparisons. *$p < 0.05$, and n.s. indicates $p > 0.05$. **D** The number of cells with p-VEGFR2 accumulation (accumulated particles bigger than 5 μm^2) among the total number of the cells was counted and shown as mean ± SE in graph **C**. N = 17, 17, 20, 18, 17, 18, 20, 19 (from 6 independent experiments) in ctrl (0, 3, 15, 30 min), KAI (0, 3, 15, 30 min), respectively. One-way ANOVA with post hoc multiple comparisons. ***$p < 0.001$ and n.s. indicates $p > 0.05$

VEGF-induced interaction between KIF13B and VEGFR2 (Supplemental Fig. S1C, D) [16]. KAI treatment reduced VEGF-induced colocalization of KIF13B and VEGFR2 (Fig. 6B), as KAI prevents the interaction between KIF13B and VEGFR2 (Supplemental Fig. S1C, D) [6]. VEGF increased colocalization of KIF13B and Rab11-mCerulean (Fig. 6C) and VEGFR2 and Rab11-mCerulean (Fig. 6D) in control cells. KAI treatment significantly reduced localization of VEGFR2 and KIF13B in Rab11-positive recycling vesicles (Fig. 6C, D).

To further study the role of Rab11-mediated slow recycling of VEGFR2, we examined the effect of knockdown of *Rab11a* on localization of VEGFR2 and p-VEGFR2 (Y1175) (Supplemental Fig. S6A). Initial phosphorylation of VEGFR2 at cell–cell junction was observed 3 min after VEGF stimulation in both control (scrambled siRNA-treated cells) and si*Rab11a*-treated cells. Phosphorylation of VEGFR2 was still observed at cell–cell junction 7 min and 15 min after VEGF stimulation in control cells, whereas such localization of p-VEGFR2 at cell–cell junction was markedly reduced by knockdown of *Rab11a* (Supplemental Fig. S6A). Note: VEGFR2 is known to be dephosphorylated before entering Rab11 recycling vesicles [13]. Thus, recycled VEGFR2 to the cell–cell junction needs to receive VEGF to be autophosphorylated again. Next, the contribution of recycled VEGFR2 on VEGF-induced permeability was examined by TEER. VEGF-induced permeability was mitigated by knockdown of *Rab11a* (Supplemental Fig. S6 B, C). The effect of knockdown of *Rab11a* phenocopied the effect of knockdown of *KIF13B* (Fig. 1A, B). In both cases, knockdown was still observed at the late time points (12 h or 18 h) (Supplemental Fig. S1A, B, and S6D, E), however, VEGF-induced permeability at a late time point was not affected by knockdown of *KIF13B* or *Rab11a* (Fig. 1A, C and Supplemental Fig. S6B). Nonetheless, the data showed that Rab11-mediated slow recycling of VEGFR2 is necessary for VEGF-induced endothelial permeability (15–30 min). In contrast, knockdown of *Rab4*, which mediates fast recycling of VEGFR2, did not affect VEGF-induced permeability (Supplemental Figure S6F, G, H, I). Knockdown of *Syntaxin 6 (STX6)*, which mediates post-Golgi trafficking of VEGFR2, also did not inhibit but rather enhanced VEGF-induced permeability (Supplemental Fig. S6F, G, H, I).

The effect of pharmacological inhibition of VEGFR2 internalization on VEGF-induced permeability was also examined (Supplemental Fig. S7). VEGFR2 is known to internalize via Clathrin-mediated endocytosis, micropinocytosis, and Caveolin-mediated endocytosis, which are inhibited by Pitstop2 [24], EIPA [25], and Filipin III [26], respectively. Pitstop2 and Filipin III only slightly inhibited VEGF-induced permeability, and they did not affect inhibitory effect of KAI (Supplemental Fig. S7A, B, C, D). In contrast, EIPA, the inhibitor for micropinocytosis, eliminated the effect of KAI (Supplemental Fig. S7E, F). In the presence of EIPA, VEGF could still induce permeability, but the timing to fully open the barrier was significantly delayed (Supplemental Fig. S7G). Taken together, KIF13B mediates recycling of internalized VEGFR2 via the micropinocytosis pathway to induce permeability in response to VEGF.

Next, we examined localization of p-VEGFR2 in late endosome and lysosome by co-immunostaining. Consistent with the observation in co-IP with Rab7 (Fig. 5E, F), p-VEGFR2 (Y1175) was highly colocalized with the late endosome marker Rab7 15 min after VEGF stimulation in KAI-treated cells (Supplemental Fig. S8). At 3 min after VEGF-A stimulation, phosphorylation of VEGFR2 was observed at cell–cell junctions in both control and KAI-treated hREC, consistent with Fig. 4. KAI treatment induced accumulation of p-VEGFR2, which was colocalized with Rab7 (Supplemental Fig. S8A, B). We further analyzed colocalization of p-VEGFR2 (Y1175) and lysosome marker LAMP2 (Fig. 7). KAI induced accumulation of p-VEGFR2 in LAMP2 positive lysosomes 15 min and 30 min after VEGF-A stimulation, compared with control (Fig. 7A, B). Together, these data show that inhibition of VEGFR2 trafficking by KAI treatment traffics VEGFR2 to late endosome and lysosome for degradation.

We also quantified the total amount of VEGFR2 after VEGF-A stimulation in control peptide-treated hREC and KAI-treated hREC (Fig. 7C, D). Compared to control, KAI treatment reduced the total amount of VEGFR2 at 15 min after VEGF-A stimulation (Fig. 7C, D). Degradation of VEGFR2 was also tested in scrambled shRNA-transduced control and shRNA-*KIF13B*-transduced cells (Fig. 7E, F). Knockdown of *KIF13B* tended to decrease the total amount of VEGFR2, although it was not statistically significant (Fig. 7E, F). These results together show that KIF13B

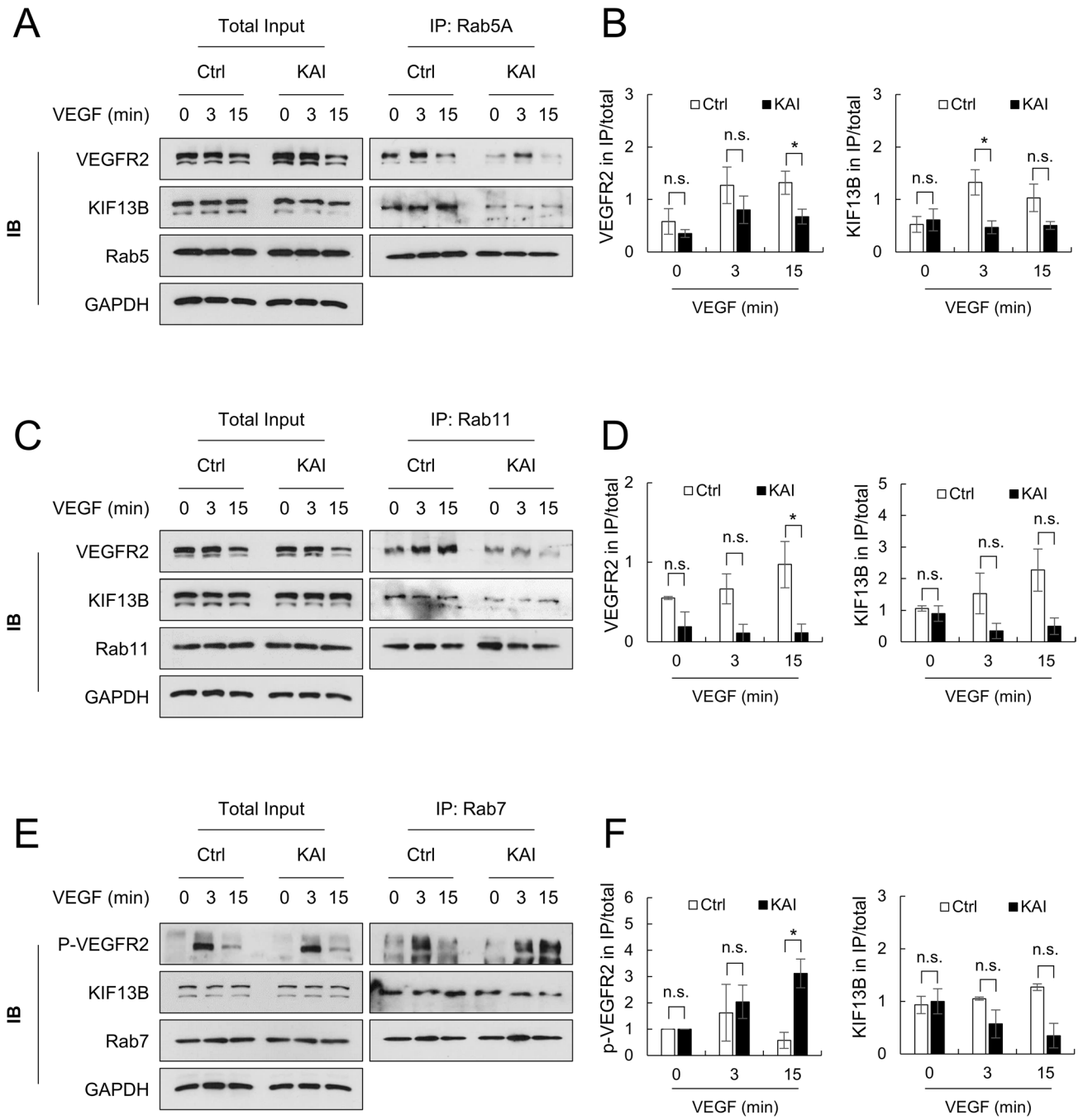

contributes to recycling of internalized VEGFR2. Inhibition of KIF13B traffics VEGFR2 to lysosomal degradation instead of recycling and limits the amount of VEGFR2 on the cell surface. Overall, the results show that VEGFR2 recycling is essential for VEGF-A signaling and endothelial permeability.

Inhibition of VEGFR2 trafficking ameliorates pathological vascular leakage

We examined whether inhibition of VEGFR2 trafficking is an effective strategy to inhibit vascular leakage in wet AMD. We tested the efficacy of KAI on laser-induced vascular leakage in the mouse model (Fig. 8). C57BL/6 mice received laser burns on Bruch's membrane, which mimics disruption of Bruch's membrane in wet AMD, and induces vascular leakage and neovascularization [27, 28]. Mice were treated with eyedrops of either control peptide or KAI (5 μg/eye in

◂**Fig. 5** Association of VEGFR2 to Rab family proteins is impaired by KAI, an inhibitor for KIF13B-mediated VEGFR2 trafficking. **A**, **B** Association of VEGFR2 and KIF13B with Rab5-positive early endosome in hREC pretreated with either scrambled control peptide or KAI (10 μM). After VEGF-A stimulation (50 ng/mL) for indicated time periods, proteins were co-immunoprecipitated (IP) with Rab5 and analyzed by western blotting. Representative blots were shown in **A**. Quantification of the proteins co-immunoprecipitated with Rab5 was normalized by proteins in the total lysate and shown as mean ± SE in the graph **B**. N = 4. Student's t test was performed for statistical analysis in ctrl and KAI groups with the same time point of VEGF stimulation. *$p < 0.05$. n.s. indicates $p > 0.05$. **C**, **D** Association of VEGFR2 and KIF13B with Rab11-positive recycling vesicles in hREC pretreated with either scrambled control peptide or KAI (10 μM). After VEGF-A stimulation (50 ng/mL) for indicated time points, proteins were co-immunoprecipitated with Rab11 and analyzed by western blotting. Representative blots were shown in **C**. Quantification of the proteins co-immunoprecipitated with Rab11 was normalized by proteins in the total lysate and shown as mean ± SE in the graph **D**. N = 4. Student's t test. *$p < 0.05$. n.s. indicates $p > 0.05$. **E**, **F** Association of phosphorylated VEGFR2 (Y1175), and KIF13B with Rab7-positive late endosome in hREC pretreated with either scrambled control peptide or KAI (10 μM). After VEGF-A stimulation (50 ng/mL) for indicated time points, proteins were co-immunoprecipitated with Rab7, and analyzed by western blotting. Representative blots were shown in **E**. Quantification of the proteins co-immunoprecipitated with Rab7 was normalized by proteins in the total lysate and shown as mean ± SE in the graph **F**. N = 4. Student's t test. *$p < 0.05$. n.s. indicates $p > 0.05$

5 μl in PBS) once a day for 3 days. Three days after laser burns, Evans blue was injected i.p. to examine the Evans blue extravasation on the following day. The control peptide-treated mice showed extravasation of Evans blue at the site with laser burn (Fig. 8A top panel). KAI treatment reduced the extravasation of Evans blue (Fig. 8A bottom panel and 8C). Laser-induced neovascularization at day 4 was also analyzed by staining with isolectin B4 (ILB4), an endothelial marker. Compared to the control mice, laser-induced neovascularization was also reduced by daily treatment with KAI, but it was not statistically significant (Fig. 8A, D). Note, neovascularization at the late stage was significantly reduced by continuous KAI treatment for 14 days [7]. As laser-induced vascular leakage also facilitated macrophage recruitment [27], we observed macrophages by staining with marker CD68 (Fig. 8B, E). Thus, it appears that KAI treatment also inhibited macrophage recruitment.

Discussion

Herein we showed that VEGF-A stimulation first induced phosphorylation of VEGFR2 at cell–cell junction. Internalized p-VEGFR2 then trafficked to Rab5 positive early endosome to induce signaling [9–11]. Our data show that KIF13B interacted with internalized VEGFR2 at Rab5-positive early endosome to escort VEGFR2 to the recycling pathway (see Fig. 8F). Blocking the interaction between VEGFR2 and KIF13B prevented VEGFR2 dephosphorylation, a necessary step for the receptor to enter the Rab11 recycling pathway [12, 13]. Thus, inhibition of VEGFR2 trafficking caused aberrant accumulation of phosphorylated VEGFR2 in lysosomes to be degraded. This recycling of VEGFR2 to the cell surface may be important in tuning VEGF signaling and regulating endothelial permeability, as both KAI treatment and knockdown of *KIF13B* inhibited VEGF-induced endothelial permeability.

Endocytosis of phosphorylated VEGFR2 is mediated by ephrin-B2, PAR-3, Dab2, and aPKC [9, 10]. Internalized VEGFR2 is then transported to early endosomes by myosin family molecular motor MYO6 and Synectin [11]. In contrast, VEGFR2 trafficking to the cell surface is mediated by KIF13B [16], t-SNARE Syntaxin 6 [14], SUMO endopeptidase SENP1 [29], and another myosin family molecular motor MYO1C [15]. The potential interaction and cooperation of KIF13B with these molecules needs further investigation. Nonetheless, we demonstrated the requisite role of KIF13B in VEGFR2 trafficking during recycling, in addition to the known role of KIF13B trafficking of newly synthesized VEGFR2 from the Golgi apparatus [16].

Failure of trafficking misdirect VEGFR2 to the degradation pathway [14–16, 30, 31]. Thus, KAI peptide decreased VEGFR2 in early endosomes and recycling endosomes and increased VEGFR2 in Rab7-positive late endosomes 15 min after VEGF-A stimulation (Fig. 5F). To keep functional VEGFR2 in the cycle, unfunctional VEGFR2 needs to be rapidly and efficiently removed to avoid disruptive signaling. Ubiquitin isopeptidase USP8 [32] and ER-resident ubiquitin E3 ligase RNF121 mediate degradation of immature VEGFR2 [33]. How failed trafficking of VEGFR2 induces its ubiquitination and subsequent degradation remains an open question.

The interaction between Rab family proteins and KIF13B or its homolog has been reported [34–36]. KIF13B interacts with the early endosome through its tail domain (832–1826 aa) [35], which includes the VEGFR2 binding domain (1238–1260 aa) and Cap-gly domain (1703–1768 aa). As internalized VEGFR2 enters Rab5-positive early endosomes [9–11], KIF13B may interact with early endosomes via VEGFR2. Alternatively, KIF13B may directly interact with Rab5 through its Cap-gly domain, as in the case of kinesin-73, *Drosophila* homolog of KIF13B [34]. In KAI-treated hRECs, association of KIF13B to Rab5-positive vesicles was not observed before and after VEGF stimulation (Fig. 5A, B). KAI also reduced VEGFR2 in co-IP with Rab5 at a later time point (15 min after VEGF stimulation). Thus, the interaction of KIF13B to early endosome likely occurs via VEGFR2, not directly through Rab5. KIF13A, the closest homolog of KIF13B, interacts with the active form of Rab11 via stalk (351–1307 aa) and tail (1307–1770 aa) [36]. Similarly, KIF13B may interact with Rab11. Alternatively,

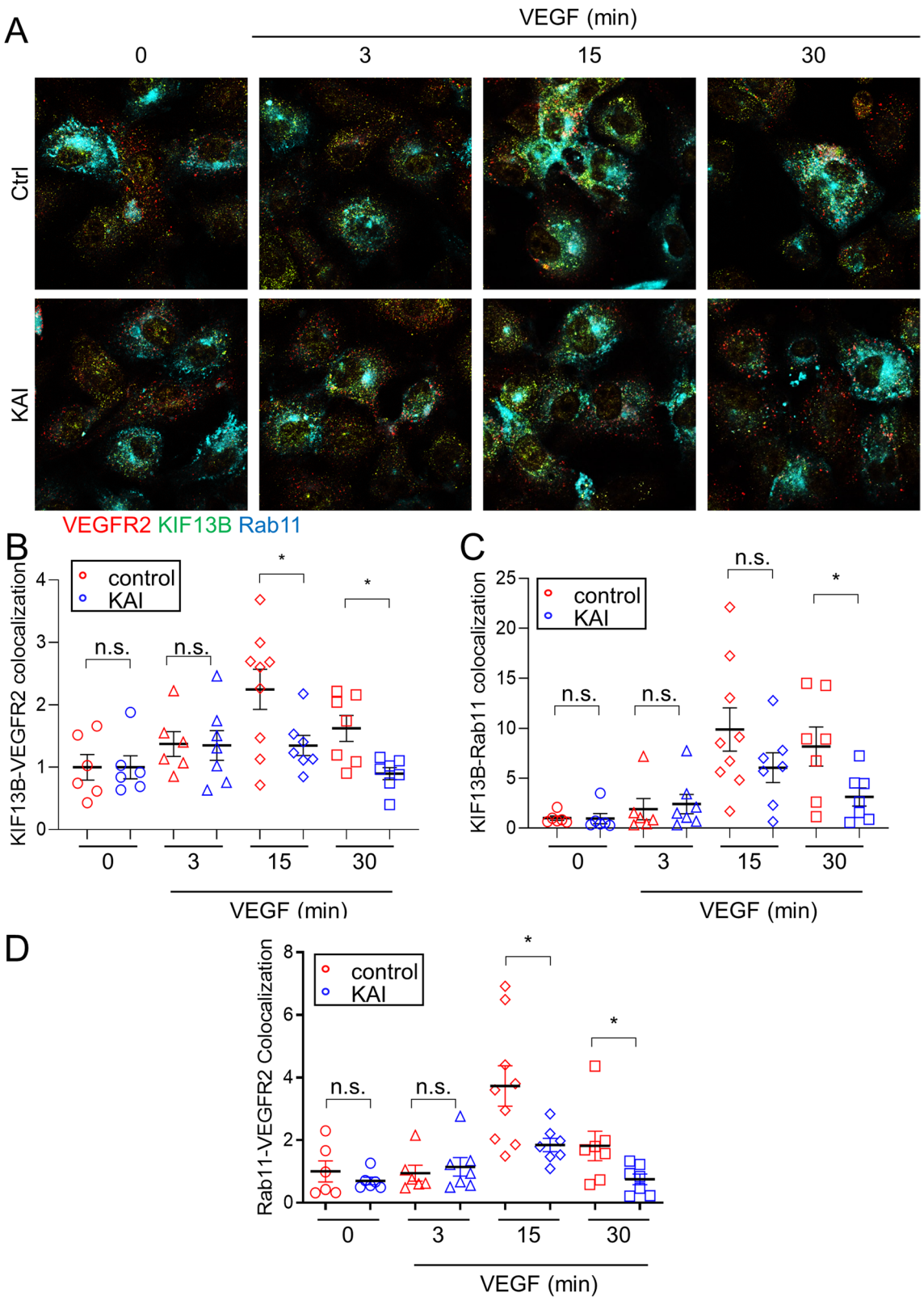

KIF13B and KIF13A may form a heterodimer [37] for the recycling of VEGFR2. It is noteworthy that KIF13B did not interact with the lysosome [35]. Together, our data show that KIF13B interacts with internalized VEGFR2 in early endosome and escorts VEGFR2 to the Rab11-mediated recycling pathway. Thus, inhibition of the function of KIF13B

◂**Fig. 6** Inhibition of KIF13B reduced association of VEGFR2 to recycling vesicle. **A**–**D** Immunostaining for VEGFR2 (red pseudo color, stained with Alexa 647) and KIF13B (green pseudo color, stained with Alexa 594) and fluorescence of mCerulean-Rab11 (cyan) in hREC pretreated with either control peptide or KAI (10 μM), and stimulated with VEGF-A (50 ng/mL) for indicated time periods. The colocalizations of KIF13B and VEGFR2, KIF13B and Rab11, VEGFR2 and Rab11 were quantified by Image J and shown as mean ± SE in graph **B**–**D**, respectively. N = 6, 6, 9, 7, 6, 7, 7, 7 for pictures (from 3 independent experiments) in ctrl (0, 3, 15, 30 min), KAI (0, 3, 15, 30 min), respectively. Student's t test. *$p < 0.05$, and n.s. indicates $p > 0.05$

prevents recycling of VEGFR2 and leads to lysosomal degradation of VEGFR2.

KAI is designed to disrupt the interaction between KIF13B and VEGFR2 [6], and KAI is specific to VEGFR2 with high affinity [7]. We observed similar defects by both KAI treatment and knockdown of KIF13B with slight differences; reduced phosphorylation of VEGFR2 at Y1175 was observed by knockdown of KIF13B, but not by KAI treatment (Fig. 2). KIF13B has multiple cargo binding domains, and previously shown to transport PIP3 [1] and hDlg [38–40]. The aforementioned possible interaction with Rab proteins [34, 36], or even function of KIF13B as a scaffolding protein (not requiring motor function) is also suggested [41]. Thus, defects seen by knockdown of *KIF13B* but not KAI treatment can be explained by VEGFR2-independent function. Although function of KIF13B on endocytosis of LRP1 was suggested in liver cells [41], endocytosis of VEGFR2 was KIF13B independent (Fig. 3E–G), and KAI treatment did not affect phosphorylation of ERK1/2 by internalized VEGFR2 (data not shown). As kinesins have multiple cargoes, it is important to inhibit trafficking of each cargo by using the dominant-negative approach, and we designed KAI for such purpose. KAI inhibited VEGF-induced endothelial permeability in vivo [17] and in laser-induced permeability, as a model of wet AMD (Fig. 8). Thus, inhibition of KIF13B-mediated VEGFR2 trafficking can provide precise understanding of regulation mechanisms of VEGF signaling by VEGFR2 trafficking as discussed below. And inhibition of VEGFR2 trafficking is also promising therapeutic strategy for cancer metastasis [17] and wet AMD [7].

Several types of VEGFR2 trafficking occur simultaneously: constitutive (ligand-independent) internalization and recycling through Rab4 or Rab11 pathways [42], VEGF-induced internalization [9, 11, 25, 43] and recycling [13]. There is a technical limitation to separating all events to see the specific one. As KIF13B has both functions of post-Golgi trafficking of VEGFR2 [16] and VEGFR2 recycling (shown in this study), the effects of KAI or knockdown of KIF13B may be due to inhibition of both post-Golgi trafficking and recycling of VEGFR2. For VEGF-induced endothelial permeability, recycling of VEGFR2 plays a major role, but not post-Golgi trafficking of newly synthesized VEGFR2, as knockdown of *Rab11* inhibited VEGF-induced permeability, but not knockdown of *Syntaxin 6* (Supplemental Fig. S6 B, C, F, G). Knockdown of *Syntaxin 6* rather enhanced VEGF-induced endothelial permeability. Probably inhibition of trafficking of newly synthesized VEGFR2 increased ratio of recycled VEGFR2/total amount of VEGFR2 on the cell surface. As the recycled VEGFR2 via the Rab11 pathway plays a major role in endothelial permeability (Supplemental Fig. S6B, C), an increased ratio of recycled VEGFR2 enhances the downstream signaling for endothelial permeability.

Internalized VEGFR2 by different pathways may play different roles in EC. VEGFR2 is known to internalize via Clathrin-mediated endocytosis [24], micropinocytosis [25], and Caveolin-mediated endocytosis [26]. None of the inhibitors prevented VEGF-induced endothelial permeability (Supplemental Fig. S7), suggesting other pathways compensate for the role when one of the pathways is inhibited. Interestingly, only EIPA, the inhibitor for micropinocytosis, eliminated the effect of KAI, and also delayed the timing of endothelial permeability (Supplemental Fig. S7E, F). In the presence of EIPA, internalized VEGFR2 via micropinocytosis is gone, while the pool of internalized VEGFR2 via Clathrin- and Caveolin-mediated endocytosis are still present. Although internalized VEGFR2 through all pathways goes to Rab5 early endosomes, only a pool of internalized VEGFR2 via micropinocytosis can be recycled by KIF13B, as the effect of KAI was eliminated only by EIPA (Schematic figure in Supplemental Fig. S9). It is still a puzzle how KIF13B can distinguish different pools of VEGFR2. There may be differences in the associated molecules with VEGFR2 in different pathways. Nonetheless, internalization of VEGFR2 via micropinocytosis is known to be crucial for downstream signaling and function in EC [44]. In this study, KAI could inhibit VEGF-induced signaling and permeability (Figs. 1, 2), suggesting that internalization via micropinocytosis and recycling of VEGFR2 plays a major role in VEGF-induced permeability. Although VEGF-induced permeability still occurred in the presence of EIPA, it took longer time to induce full opening of the endothelial barrier (Supplemental Fig. S7), also suggesting the importance of internalized VEGFR2 via micropinocytosis. It is still unknown how other pools of internalized VEGFR2 (after Clathrin- and Caveolin-mediated endocytosis) are recycled, and how such recycled VEGFR2 can compensate for the role of recycled VEGFR2 via micropinocytosis/Rab11 pathway.

Regarding the timeframe of internalization and recycling, activation of ERK1/2 by internalized VEGFR2 is observed 2–5 min after VEGF stimulation [45]. Colocalization of internalized VEGFR2 with Rab5 was examined 10 min [46] or 15 min after VEGF stimulation [31]. Our data showed their interaction even earlier, 3 min after VEGF stimulation (Fig. 5A, B). After that, dephosphorylated VEGFR2 is sent to Rab11-mediated recycling endosomes 15–30 min after

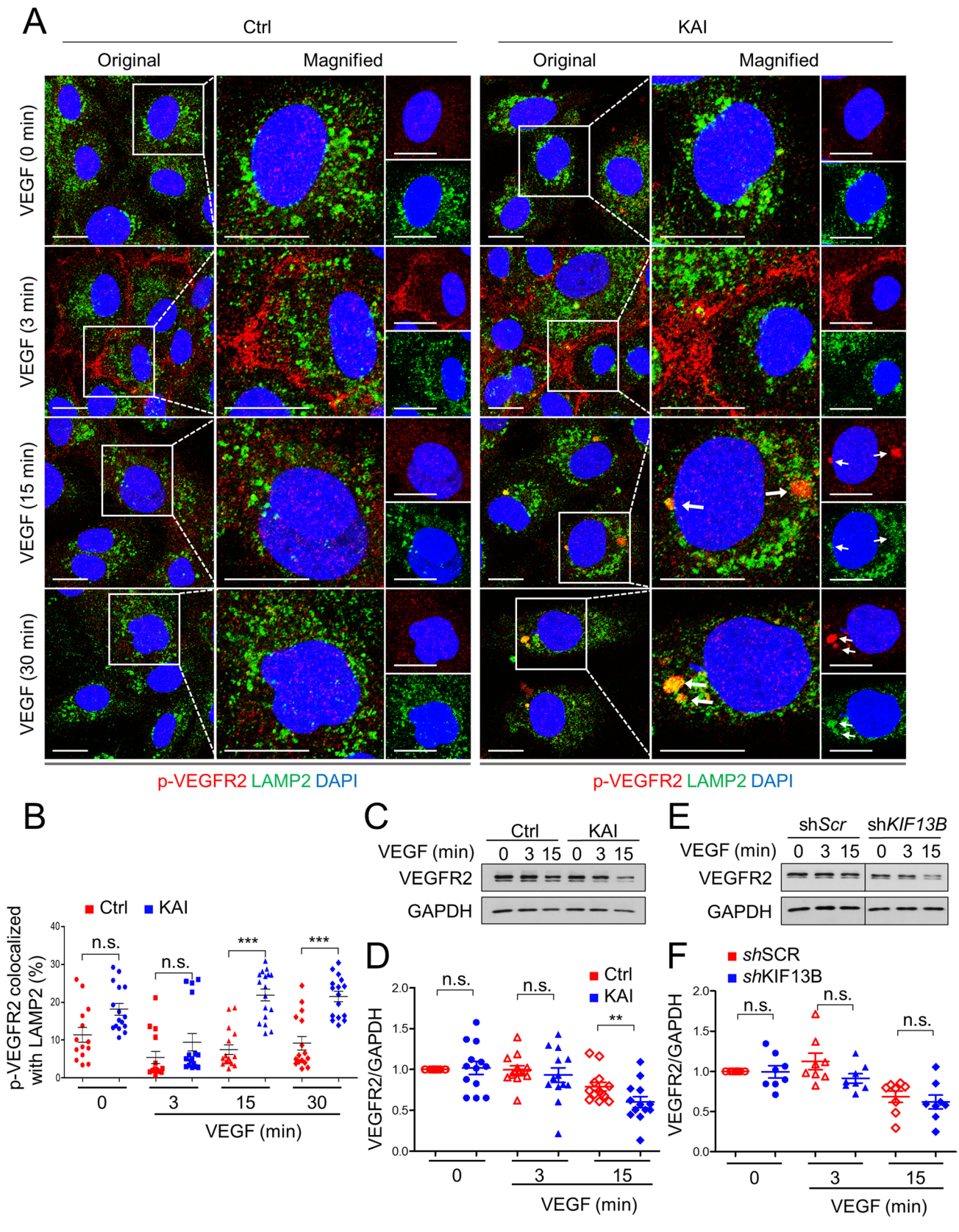
A
Ctrl
KAI
Original
Magnified
Original
Magnified
VEGF (0 min)
VEGF (3 min)
VEGF (15 min)
VEGF (30 min)
p-VEGFR2 LAMP2 DAPI
p-VEGFR2 LAMP2 DAPI
B
Ctrl
KAI
p-VEGFR2 colocalized with LAMP2 (%)
n.s.
n.s.
***
***
0
3
15
30
VEGF (min)
C
Ctrl
KAI
VEGF (min)
0 3 15 0 3 15
VEGFR2
GAPDH
D
Ctrl
KAI
VEGFR2/GAPDH
n.s.
n.s.
**
0
3
15
VEGF (min)
E
shScr
shKIF13B
VEGF (min)
0 3 15 0 3 15
VEGFR2
GAPDH
F
shSCR
shKIF13B
VEGFR2/GAPDH
n.s.
n.s.
n.s.
0
3
15
VEGF (min)

◂**Fig. 7** Failure of VEGFR2 trafficking sends p-VEGFR2 to lysosome. **A** Immunostaining for p-VEGFR2 (Y1175, red) and LAMP2 (green) in hREC pretreated with either control peptide or KAI (10 μM), and stimulated with VEGF-A (50 ng/mL) for indicated time periods. Scale bars; 10 μm. **B** The colocalization of p-VEGFR2 and LAMP2 was quantified by Image J and shown as mean ± SE in graph **B**. N = 14, 16, 15, 16, 16, 17, 16 and 16 for pictures in ctrl (0, 3, 15, 30 min), KAI (0, 3, 15, 30 min), respectively, from 3 independent experiments. One-way ANOVA with post hoc multiple comparisons. ***$p < 0.001$ and n.s. indicates $p > 0.05$. **C**, **D** Degradation of VEGFR2 after VEGF-A stimulation (50 ng/mL) in hREC treated with either scrambled control peptide or KAI peptide (10 μM). Representative blots were shown in C. Quantification of VEGFR2 was normalized by loading control GAPDH, and shown in graph D as mean ± SE. N = 13. T test was performed for statistical analysis in ctrl and KAI groups with the same time point of VEGF stimulation. **$p < 0.01$. **E**, **F** Degradation of VEGFR2 after VEGF-A stimulation (50 ng/mL) in hREC transduced with scrambled shRNA or shRNA-*KIF13B*. Representative blots were shown in **E**. Intensity of the bands of VEGFR2 was normalized by loading control GAPDH, and shown in graph **F** as mean ± SE. N = 8. T test was performed for statistical analysis in scrambled shRNA and shRNA-*KIF13B* groups with the same time point of VEGF stimulation. *N.s.* no significant difference

VEGF stimulation (Fig. 6D), which is consistent with previous papers showing colocalization of VEGFR2 with Rab11 30 min after VEGF stimulation [13, 31, 46]. Recycling of VEGFR2 to the cell surface can occur within 10–20 min [42], with a half-time of approximately 12–15 min [47, 48]. Inhibition of KIF13B-mediated VEGFR2 trafficking reduced cell surface VEGFR2 15–30 min after VEGF stimulation (Fig. 3A, B). This timeframe fits the recycling of VEGFR2 [42, 47, 48]. In contrast, release of VEGFR2 from Golgi was observed ~ 30 min after VEGF stimulation [14, 16, 49]. Post-Golgi trafficking of VEGFR2 may take longer time but induces further expression of VEGFR2 and restore the amount of VEGFR2 on the cell surface, as part of VEGFR2 is degraded after VEGF stimulation [16]. Both recycling of VEGFR2 and post-Golgi trafficking are required for continuous activation of VEGFR2 [13, 16], however, possibly mediate different downstream events, as knockdown of *Syntaxin 6* did not block VEGF-induced endothelial permeability (Supplemental Fig. S6F, G).

Then, what is the function of slow recycling of VEGFR2 through Rab11 pathway? Rab4-mediated fast recycling can bring VEGFR2 to the cell surface while being still phosphorylated [13, 31], so that recycled p-VEGFR2 can immediately activate local signaling. In contrast, VEGFR2 needs to be dephosphorylated to enter Rab11-mediated slow recycling pathway [13], and then be further phosphorylated again after recycling to the cell surface for the next cycle. Knockdown of *Rab11* reduced phosphorylated VEGFR2 at the cell–cell junction 7–15 min after VEGF stimulation (Supplemental Fig. S6A), suggesting recycling of VEGFR2 via Rab11 pathway can contribute to maintaining VEGF signaling at the cell–cell junction at 7–15 min after VEGF stimulation. Keeping phosphorylated VEGFR2 at cell–cell junction or fast-recycling of phosphorylated VEGFR2 would be faster and simpler than internalization of phosphorylated VEGFR2 followed by dephosphorylation, recycling via Rab11 pathway, and phosphorylation again. However, VEGF-induced endothelial permeability needs Rab11-mediated slow recycling of VEGFR2, not Rab4-mediated fast recycling (Supplemental Fig. S6B, C, F, G). Maybe slow recycling of VEGFR2 plays a role in recruiting downstream signaling molecules from cytosol to the specific area of the plasma membrane. It needs further investigation in the future. VEGFR2 trafficking seems to regulate selective downstream events, among the multiple signaling events induced by VEGF/VEGFR2. Interestingly, co-receptor of VEGFR2, NRP1, is required for escorting VEGFR2 to Rab11-mediated recycling pathway [13], and VEGF-induced endothelial permeability [27]. These findings also suggest importance of Rab11-mediated slow recycling of VEGFR2 to regulate endothelial permeability.

Our previous studies showed that KIF13B-mediated VEGFR2 trafficking regulated EC migration and sprouting angiogenesis [16] and VEGF-induced vascular leakage over periods of up to weeks [17]. The present results, however, show a rapid response to VEGF-A occurring within 3 min. As shown in the present study, the interaction between VEGFR2 in the early endosomes with molecular motors KIF13B and MYO1C restore VEGFR2 at the cell surface within minutes. Kinesins transport their cargo for 50–200 mm per day [50], that is, 35–140 μm/min. The speed of kinesins is sufficiently rapid to transport cargo to the cell surface within minutes in endothelial cells (50–70 μm diameter). Thus, recycled VEGFR2 by KIF13B can induce downstream signaling, such as SRC-mediated phosphorylation of VE-cadherin (15 min) and endothelial permeability (15–30 min). However, inhibitory effect of KAI on phosphorylation of VEGFR2 specifically at Y951 (3 min) cannot be explained by inhibition of VEGFR2 recycling, as this timeframe is likely before recycling.

Then, how is VEGF signaling regulated by VEGFR2 trafficking? Abrogation of KIF13B-mediated VEGFR2 trafficking reduced phosphorylation of VEGFR2 greater degree at Y951 than Y1175 sites, even though the initial cell-surface VEGFR2 levels were not altered. VEGF stimulation simultaneously induces auto-phosphorylation of VEGFR2 at multiple tyrosine residues, Y951, Y1054/1059, Y1175, and Y1214 [51]. Each phosphorylation site has unique function to induce VEGFR2 activation or downstream signaling pathways. Phosphorylation at Y1175 regulates cell migration, proliferation, and homeostasis, whereas phosphorylation at Y951 regulates permeability and survival [8]. Autophosphorylation at Y1054/1059 indicates dimerization of VEGFR2 and activation of its kinase activity[52]. Phosphorylation of VEGFR2 at Y1059 3 min after VEGF stimulation was not inhibited by KAI treatment (Supplemental Fig. S2B,

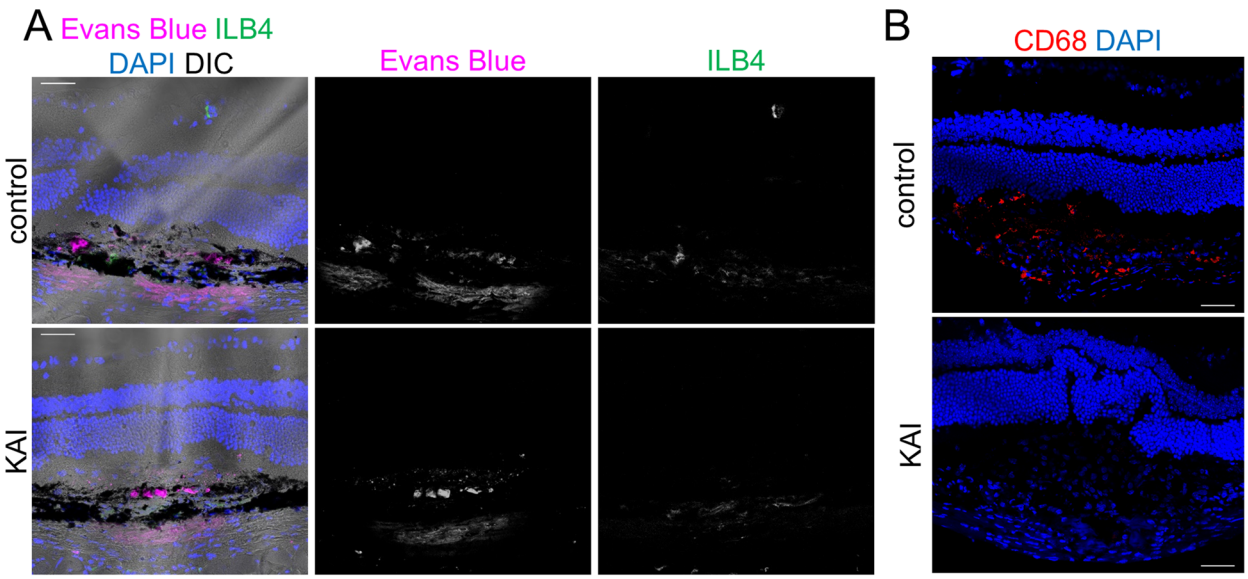
A Evans Blue ILB4
DAPI DIC
Evans Blue
ILB4
control
KAI
B
CD68 DAPI
control
KAI

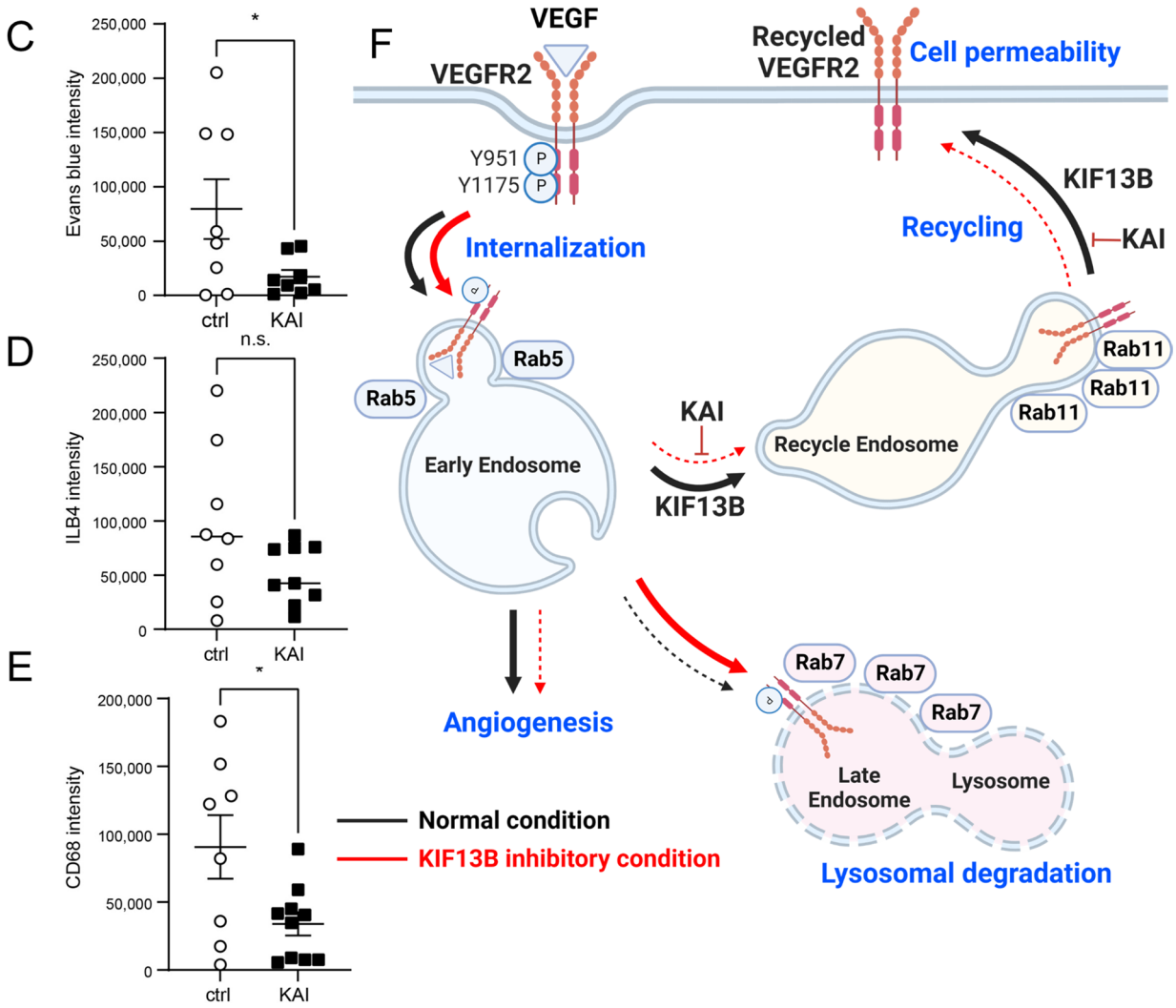
C
Evans blue intensity
250,000
200,000
150,000
100,000
50,000
0
ctrl
KAI
*
n.s.
D
ILB4 intensity
E
CD68 intensity
F
VEGF
VEGFR2
Y951
Y1175
P
Internalization
Recycled VEGFR2
Cell permeability
KIF13B
KAI
Recycling
Rab5
Early Endosome
Recycle Endosome
Rab11
Angiogenesis
Rab7
Late Endosome
Lysosome
Lysosomal degradation
Normal condition
KIF13B inhibitory condition

◂**Fig. 8** Pharmacological inhibition of VEGFR2 trafficking ameliorates vascular leakage in mice. **A**–**E** Effects of KAI eyedrop on the pathological vascular leakage in mice. After receiving laser burns, mice were treated either control peptide (ctrl) or KAI (5 µg/eye in 5 µl PBS) daily. On day 3, Evans blue was injected i.p., and Evans blue leakage was measured 24 h after injection. Cryosections of the damaged area were also stained with ILB4 (**A**) and CD68 (**B**) to visualize neovascularization and macrophage recruitment, respectively. Representative images were shown in **A** and **B**. Scale bars; 50 µm. The intensity of the Evans blue extravasation, ILB4, and CD68 was quantified and shown in the graph as mean ± SE in **C**–**E**. N = 8 and 10 for ctrl and KAI, respectively. **F** Schematic showing the working model in this study. VEGF induces internalization of phosphorylated VEGFR2 to Rab5-positive early endosomes. Dephosphorylated VEGFR2 is transferred to Rab11-positive recycling vesicle by KIF13B and further trafficked to the cell surface. When KIF13B function is blocked by either knockdown or pharmacological inhibitor KAI, VEGFR2 trafficking is failed, and phosphorylated VEGFR2 is sent from early endosomes to late endosome and lysosome for degradation. Recycling of VEGFR2 is required for VEGF-induced signaling for endothelial permeability. Thus, this pathway can be a therapeutic target for vascular leakage-related diseases such as wet AMD

C), thus the reduced phosphorylation at Y951 by KAI or knockdown of KIF13B is not due to defects in dimerization nor reduced kinase activity. Rather, selective dephosphorylation is possible, as suggested by other research groups [43, 53–55]. Dephosphorylation of VEGFR2 is mediated by multiple phosphatases with overlapping and preferred target residues. Cell membrane phosphatase vascular endothelial protein Tyr phosphatases (VE-PTPs) dephosphorylates both Y951 and Y1175 of VEGFR2 [51]. Intracellular phosphatases SRC homology-2 domain-containing phosphatase 1 (SHP1) dephosphorylates Y1175 and Y1054/59, but not Y951 [51]. In contrast, SHP2 dephosphorylates VEGFR2 at Y951, Y996, and Y1059, but not Y1175 [55]. Regulation of phosphorylation status of VEGFR2 by its trafficking has been demonstrated [11, 31, 43, 46, 56]. When trafficking of internalized VEGFR2 from periphery to early endosome is inhibited, VEGFR2 can be dephosphorylated by membrane phosphatases [11, 46]. Similarly, when recycling of internalized VEGFR2 is inhibited, VEGFR2 can be dephosphorylated by intracellular phosphatases [31]. In this study, we showed reduced phosphorylation of Y951 3 min after VEGF stimulation by inhibition of KIF13B function mediating VEGFR2 trafficking, whereas phosphorylation of Y1175 was sustained. The timeframe is before recycling. Selective dephosphorylation of Y951, 5 min after VEGF stimulation, was also observed by knockdown of *Syndecan-2* [43]. Syndecan-2 regulates the internalization of DEP1, which selectively dephosphorylates Y951 of VEGFR2. Increased cell surface DEP1 by knockdown of *Syndecan-2* promotes dephosphorylation of Y951 of VEGFR2 [43]. Similarly, inhibition of KIF13B may keep VEGFR2 in close contact with phosphatases such as DEP1. The mechanisms of how KIF13B-mediated VEGFR2 trafficking affects potential interaction with selective phosphatases, and whether it is SHP2 or DEP1 need further investigation in the future.

An alternative possibility is failure of VEGFR2 recycling reduces the amount of VEGFR2 at the cell surface to be ligated with VEGF. Impaired VEGFR2 trafficking caused accumulation and degradation of VEGFR2 in lysosomes. Thus, VEGF signaling was reduced and release of VEGFR2 from the perinuclear pool was inhibited. Both inhibition of VEGFR2 trafficking from the recycling pool and the newly synthesized pool prevented VEGF signaling, thereby inhibiting downstream signaling mediating endothelial permeability. Thus, targeting VEGFR2 trafficking is potentially a promising anti-endothelial permeability strategy.

Materials and methods

Antibodies and reagents

Rabbit antibodies against VEGFR2, p-VEGFR2 (Y1175), p-VEGFR2 (Y951), p-VEGFR2 (Y1059), SRC, p-SRC (Y416), Rab7, Rab11, CD68 were from Cell Signaling Technology (Danvers, MA, USA). Rabbit antibodies against KIF13B and p-VE-cadherin (Y658) were from Invitrogen (Carlsbad, CA, USA), p-VE-cadherin (Y685), VE-cadherin and Rab5 were from Abcam (Cambridge, MA, USA). Rabbit antibodies against Rab11 (Proteintech, Rosemont, IL) and GAPDH (Sigma-Aldrich, St. Louis, MO, USA) were also used. The goat antibody against VEGFR2 was from R&D Systems (Minneapolis, MN). Mouse antibodies against VE-cadherin, Rab4 (Santa Cruz, Dallas, TX), Rab5A, Rab7 (Cell Signaling), Syntaxin 6, EEA1, and LAMP2 (BD Bioscience, Franklin Lakes, NJ, USA), EXOC6 (Sigma) were also used. Mouse monoclonal antibody against KIF13B was kindly provided by Dr. Toshihiko Hanada [1, 37] (Tufts University, Boston, USA). Other reagents used were ILB4 (Vector Laboratories, Burlingame, CA, USA), Alexa 594 anti-rabbit antibody, Alexa 488 anti-mouse antibody, Alexa 488 anti-goat antibody, Alexa 488-streptavidin (Invitrogen), and HRP-conjugated secondary antibodies (Jackson Immunoresearch Laboratories, West Grove, PA, USA). Recombinant human VEGF-A^{165} was purchased from Peprotech (Cranbury, NJ, USA). Pharmacological inhibitors, EIPA, Filipin III, Pitstop2 were from Cayman Chemical (Ann Arbor, MI). Silencer Select siRNA for human Rab4A (S224510), Rab11a (S16702), Syntaxin 6 (S19959), negative control siRNA were from Invitrogen. Lipofectamine RNAi max (Invitrogen) was used according to manufactures' procedure.

Cell culture

Human retinal endothelial cells (hRECs) (Cell Systems, Kirkland, WA, USA) were maintained with EGM2

MV supplemented with 5% FBS (Lonza Group, Basel, Switzerland).

Plasmids and lentivirus preparation

Lentiviruses encoding shRNA for human *KIF13B* and scrambled shRNA were as described [16]. mCerulean-Rab11a cDNA in mammalian expression vector was purchased from Addgene (Watertown MA), and subcloned into LeGo vector (Addgene). LeGo-mCerulean-Rab11a was transfected with pMD1G-VSV-G and pCMV-dr8.74G/P into HEK293T17 (ATCC, Manassas, VA) to produce lentivirus particles. Titer of the lentiviruses was measured with a lentivirus titration kit (Takara Bio USA, San Jose, CA, USA). The same multiplicity of infection (MOI) of lentiviruses encoding scrambled shRNA and shRNA-*KIF13B* (MOI 100) were used for hREC. 72 h after infection, cells were used for experiments.

Peptides

Biotin-KAI was as described [6, 7] Biotin-tagged scrambled KAI was also designed (TFLTLRDRRSHLPGVSQVPIEVV) and synthesized by a custom synthesized service (Thermo Fisher Scientific, Waltham, MA, USA) and used as control peptide.

Transendothelial electrical resistance (TEER) assay

To examine the function of KIF13B to regulate VEGF-induced endothelial barrier relaxation, transendothelial electrical resistance (TEER) was measured by electrical cell-substrate impedance sensing (ECIS, Applied BioPhysis inc, Troy, NY). Briefly, hRECs were infected with lentiviruses encoding shRNA-*KIF13B* or scrambled shRNA, and seeded in the 0.1% gelatin-coated electrode chamber (8W10E + C) as 4×10^4 cells/well. TEER was measured every 30 s overnight (4000 Hz of frequency) to monitor barrier relaxation by VEGF-A (50 ng/mL). Resistance was normalized by the resistance at time zero (when VEGF-A was added) and shown in the graphs.

To examine the effect of KAI treatment, confluent hRECs in the electrode chamber were pretreated with either control peptide or KAI peptide (10 μM) for 2 h in the complete culture medium. The change of TEER by VEGF-A (50 ng/mL) was measured as described above. Similarly, the effects of pharmacological inhibitors were tested by pretreatment of confluent hREC with inhibitors or DMSO vehicle (< 0.01%) for 2 h followed by VEGF stimulation.

Western blotting analysis

Confluent hRECs were treated with either control peptide (ctrl) or KAI (10 μM) for 2 h in the serum starvation media. After stimulation with 50 ng/mL of VEGF-A for indicated time points, cells were lysed by RIPA lysis buffer (Cell Signaling) supplemented with 10 mM sodium fluoride (Sigma), 1 mM sodium orthovanadate (Sigma), 1 mM beta-glycerophosphate (Sigma), and protease inhibitor cocktail (Sigma). Protein concentrations were measured by BCA protein assay kit (ThermoFisher), equal amounts of proteins were analyzed for western blotting. The intensity of the bands was quantified with Image Studio Lite software (LI-COR, Lincoln, NE, USA).

Immunostaining

Confluent hRECs in 0.1% gelatin-coated EZ slide 4-well chamber (Millipore, Burlington, MA, USA) were pretreated with either scrambled or KAI peptides in serum starvation media for 2 h. After stimulation with VEGF-A (50 ng/mL) for the indicated time points, cells were fixed with 4% PFA for 20 min at room temperature. Cells were permeabilized with 0.1% triton-X, and incubated with 4% BSA, 10% normal serum for the host of secondary antibodies in PBS 0.1% Tween 20. Cells were incubated with specific primary antibodies overnight, followed by incubation with fluorescently labeled secondary antibodies with Alexa-594 and Alexa-488 (Invitrogen). Stained cells were observed under a Zeiss confocal LSM 880 META with 63 × oil immersion objective lens. The confocal images were all obtained in the same microscope settings, such as gain and scanning time. The intensity was quantified with Image J (NIH).

For staining of cell surface VEGFR2, confluent hREC were fixed with 1.3% PFA for 4 min at room temperature followed by washing twice with PBS, quenching with 50 mM ammonium chloride for 2 min and washing twice with PBS. Without permeabilization, cells were incubated with 4% BSA, 10% normal serum in PBS for 1 h at room temperature, followed by incubation with antibodies in 4% BSA in PBS.

Cell surface biotinylation studies

To measure the cell surface pool of VEGFR2, we covalently labeled cell-surface proteins using a membrane-impermeable biotinylation reagent (NHS-SS-biotin; Thermo Fisher) as described previously [16] Total cell proteins and biotinylated surface proteins were analyzed by western blotting using anti-VEGFR2 antibody.

Biotinylation of internalized VEGFR2

For assessment of the internalized pool of VEGFR2 after VEGF stimulation, biotinylation of cell surface proteins was performed before VEGF-A stimulation as described [22]. Briefly, after serum starvation for 2 h, cells were incubated 0.2 mg/mL of sulfo-NHS-SS-biotin for 20 min at 4 °C. After biotin labeling on the surface proteins, cells were stimulated with VEGF-A (50 ng/mL) for indicated time points. Cells were washed with cold PBS, and cell surface biotin was cleaved off by incubating the cells on ice with 100 mM of membrane-impermeable reducing agent MESMA (2-mercaptoethane sulphonic acid (Sigma) as described [22]. Cells were lysed with lysis buffer (10 mM HEPES, 150 mM NaCl, 1% TritonX100, 0.5% NP40, 1 mM EGTA, 1 mM EDTA, 10 mM sodium fluoride, 1 mM sodium orthovanadate, 1 mM beta-glycerophosphate, and protease inhibitor cocktail). Equal amounts of protein lysates were precipitated with streptavidin-agarose beads. After washing the beads extensively with lysis buffer, proteins were analyzed by western blotting.

Co-immunoprecipitation (co-IP)

After stimulation of the cells with VEGF-A (50 ng/mL) for indicated time points, cells were lysed with IP-lysis buffer (50 mM HEPES pH 7.4, 150 mM NaCl, 2.5 mM EDTA, 0.25% NP40, 2.5% glycerol, protease inhibitor cocktail, 1 mM β-glycerophosphate, 10 mM sodium fluoride, 1 mM sodium orthovanadate). Total protein lysates were precleared with normal IgG conjugated with agarose (Santa Cruz) for 1 h at 4 °C, then proceeded for co-IP with specific antibodies (Rab5A, Rab 11 and Rab7) and Protein A/G bead (Thermo Fisher) for overnight at 4 °C. After washing with IP-lysis buffer with reduced detergent (0.025% NP40), proteins co-immunoprecipitated with Rab family antibodies were analyzed by western blotting.

Laser-induced vascular leakage

Under anesthesia, C57BL/6 received the laser burns as described [7]. Mice received eyedrop of either KAI (5 µg/eye in 5 µL PBS) or ctrl (5 µg/eye) daily on the eyes with laser burns from day 0 to day 3. On day 3 post-lasering, 250 µL of Evans blue (1% in saline) was injected i.p. Eyes were isolated 24 h later, fixed in 2% paraformaldehyde (PFA) for 30 min and frozen in optimal cutting density compound (OCT) (Sakura Finetek USA, Torrance, CA, USA) in 2 methyl 1 butane in liquid nitrogen. Cryosections of the damaged area were stained with biotinylated ILB4 followed by Alexa 488-streptavidin, or CD68 antibody and Alexa 594-anti-rabbit antibody and counterstained with DAPI. The intensity of Evans blue, ILB4, CD68 was measured using Image J and plotted in the graph using GraphPad Prism 9 (GraphPad, San Diego, CA, USA).

Statistical analysis

Data were analyzed with GraphPad Prism 9 (GraphPad). Two samples were compared by Student's *t* test. More than 2 samples were analyzed by one-way analysis of variance (ANOVA), followed by post hoc comparisons.

Supplementary Information The online version contains supplementary material available at https://doi.org/10.1007/s00018-023-04752-5.

Acknowledgements We thank Dr. Toshihiko Hanada (Tufts University, Boston, MA, USA) for sharing a monoclonal antibody against KIF13B [1]. Portions of this work were carried out in the Fluorescent Imaging Core via the Research Resources Center (RRC) at the University of Illinois at Chicago (UIC). Schematic figures are created with BioRender.com.

Author contributions: Conceptualization: H-DC, KHY. Methodology: H-DC, NTTN, KHY. Investigation: H-DC, NTTN, CZ, KT, NAS, TN. Visualization: H-DC, NTTN, CZ, KT, NAS. Funding acquisition: H-DC, TN, KHY. Project administration: KHY. Supervision: KHY. Writing—original draft: H-DC, KHY. Writing—review and editing: NTTN, KHY. Data and materials availability: The authors declare that the data supporting the findings of this study are available within the paper and its Supplementary materials. Further information and requests for resources and reagents should be directed to and will be fulfilled by the Lead Contact, Kaori Yamada (horiguch@uic.edu).

Funding This work was supported by NIH R01EY029339 (KHY), Basic Science Research Program through the National Research Foundation of Korea (NRF) funded by the Ministry of Education (2021R1A6A3A03044037) to HDC, and a core grant NIH P30EY001792 to the Department of Ophthalmology.

Data and materials availability The authors declare that the data supporting the findings of this study are available within the paper and its Supplementary materials. Further information and requests for resources and reagents should be directed to and will be fulfilled by the Lead Contact, Kaori Yamada (horiguch@uic.edu).

Declarations

Conflict of interest Authors have no conflict of interests that might be perceived to influence the results and/or discussion reported in this article.

Ethics approval All animal experiments were carried out in compliance with the relevant laws, and institutional guidelines and were approved by the Animal Care Committees administered through the Office of Animal Care and Institutional Biosafety at the University of Illinois at Chicago.

References

1. Horiguchi K, Hanada T, Fukui Y, Chishti AH (2006) Transport of PIP3 by GAKIN, a kinesin-3 family protein, regulates neuronal

cell polarity. J Cell Biol 174:425–436. https://doi.org/10.1083/jcb.200604031
2. Claesson-Welsh L, Dejana E, McDonald DM (2020) Permeability of the endothelial barrier: identifying and reconciling controversies. Trends Mol Med 27:314–331. https://doi.org/10.1016/j.molmed.2020.11.006
3. Duong CN, Vestweber D (2020) Mechanisms ensuring endothelial junction integrity beyond VE-cadherin. Front Physiol 11:519. https://doi.org/10.3389/fphys.2020.00519
4. Eelen G, Treps L, Li X, Carmeliet P (2020) Basic and therapeutic aspects of angiogenesis updated. Circ Res 127:310–329. https://doi.org/10.1161/circresaha.120.316851
5. Apte RS, Chen DS, Ferrara N (2019) VEGF in signaling and disease: beyond discovery and development. Cell 176:1248–1264. https://doi.org/10.1016/j.cell.2019.01.021
6. Yamada KH, Kang H, Malik AB (2017) Antiangiogenic therapeutic potential of peptides derived from the molecular motor KIF13B that transports VEGFR2 to plasmalemma in endothelial cells. Am J Pathol 187:214–224. https://doi.org/10.1016/j.ajpath.2016.09.010
7. Waters SB, Zhou C, Nguyen T et al (2021) VEGFR2 trafficking by KIF13B is a novel therapeutic target for wet age-related macular degeneration. Invest Ophth Vis Sci 62:5. https://doi.org/10.1167/iovs.62.2.5
8. Simons M, Gordon E, Claesson-Welsh L (2016) Mechanisms and regulation of endothelial VEGF receptor signalling. Nat Rev Mol Cell Bio 17:611–625. https://doi.org/10.1038/nrm.2016.87
9. Nakayama M, Nakayama A, van Lessen M et al (2013) Spatial regulation of VEGF receptor endocytosis in angiogenesis. Nat Cell Biol 15:249–260. https://doi.org/10.1038/ncb2679
10. Sawamiphak S, Seidel S, Essmann CL et al (2010) Ephrin-B2 regulates VEGFR2 function in developmental and tumour angiogenesis. Nature 465:487–491. https://doi.org/10.1038/nature08995
11. Lanahan AA, Hermans K, Claes F et al (2010) VEGF receptor 2 endocytic trafficking regulates arterial morphogenesis. Dev Cell 18:713–724. https://doi.org/10.1016/j.devcel.2010.02.016
12. Lanahan AA, Lech D, Dubrac A et al (2014) PTP1b is a physiologic regulator of vascular endothelial growth factor signaling in endothelial cells. Circulation 130:902–909. https://doi.org/10.1161/circulationaha.114.009683
13. Ballmer-Hofer K, Andersson AE, Ratcliffe LE, Berger P (2011) Neuropilin-1 promotes VEGFR-2 trafficking through Rab11 vesicles thereby specifying signal output. Blood 118:816–826. https://doi.org/10.1182/blood-2011-01-328773
14. Manickam V, Tiwari A, Jung JJ et al (2011) Regulation of vascular endothelial growth factor receptor 2 trafficking and angiogenesis by Golgi localized t-SNARE syntaxin 6. Blood 117:1425–1435. https://doi.org/10.1182/blood-2010-06-291690
15. Tiwari A, Jung JJ, Inamdar SM et al (2013) The myosin motor Myo1c is required for VEGFR2 delivery to the cell surface and for angiogenic signaling. Am J Physiol Heart Circ Physiol 304:H687–H696. https://doi.org/10.1152/ajpheart.00744.2012
16. Yamada KH, Nakajima Y, Geyer M et al (2014) KIF13B regulates angiogenesis through Golgi to plasma membrane trafficking of VEGFR2. J Cell Sci 127:4518–4530. https://doi.org/10.1242/jcs.156109
17. Waters SB, Dominguez JR, Cho H-D et al (2021) KIF13B-mediated VEGFR2 trafficking is essential for vascular leakage and metastasis in vivo. Life Sci Alliance 5:e202101170. https://doi.org/10.26508/lsa.202101170
18. Smith R, Ninchoji T, Gordon E et al (2020) Vascular permeability in retinopathy is regulated by VEGFR2 Y949 signaling to VE-cadherin. Elife 9:e54056. https://doi.org/10.7554/elife.54056
19. Orsenigo F, Giampietro C, Ferrari A et al (2012) Phosphorylation of VE-cadherin is modulated by haemodynamic forces and contributes to the regulation of vascular permeability in vivo. Nat Commun 3:1208. https://doi.org/10.1038/ncomms2199
20. Adam AP, Sharenko AL, Pumiglia K, Vincent PA (2010) Src-induced tyrosine phosphorylation of VE-cadherin is not sufficient to decrease barrier function of endothelial monolayers. J Biol Chem 285:7045–7055. https://doi.org/10.1074/jbc.m109.079277
21. Wessel F, Winderlich M, Holm M et al (2014) Leukocyte extravasation and vascular permeability are each controlled in vivo by different tyrosine residues of VE-cadherin. Nat Immunol 15:223–230. https://doi.org/10.1038/ni.2824
22. Nitzsche A, Pietilä R, Love DT et al (2021) Paladin is a phosphoinositide phosphatase regulating endosomal VEGFR2 signalling and angiogenesis. Embo Rep 22:e50218. https://doi.org/10.15252/embr.202050218
23. Stenmark H (2009) Rab GTPases as coordinators of vesicle traffic. Nat Rev Mol Cell Bio 10:513–525. https://doi.org/10.1038/nrm2728
24. Zhu W, Shi DS, Winter JM et al (2017) Small GTPase ARF6 controls VEGFR2 trafficking and signaling in diabetic retinopathy. J Clin Invest 127:4569–4582. https://doi.org/10.1172/jci91770
25. Basagiannis D, Zografou S, Murphy C et al (2016) VEGF induces signalling and angiogenesis by directing VEGFR2 internalisation through macropinocytosis. J Cell Sci 129:4091–4104. https://doi.org/10.1242/jcs.188219
26. Lampugnani MG, Orsenigo F, Gagliani MC et al (2006) Vascular endothelial cadherin controls VEGFR-2 internalization and signaling from intracellular compartments. J Cell Biol 174:593–604. https://doi.org/10.1083/jcb.200602080
27. Fantin A, Lampropoulou A, Senatore V et al (2017) VEGF165-induced vascular permeability requires NRP1 for ABL-mediated SRC family kinase activation. J Exp Med 214:1049–1064. https://doi.org/10.1084/jem.20160311
28. Gong Y, Li J, Sun Y et al (2015) Optimization of an image-guided laser-induced choroidal neovascularization model in mice. PLoS ONE 10:e0132643. https://doi.org/10.1371/journal.pone.0132643
29. Zhou HJ, Xu Z, Wang Z et al (2018) SUMOylation of VEGFR2 regulates its intracellular trafficking and pathological angiogenesis. Nat Commun 9:3303. https://doi.org/10.1038/s41467-018-05812-2
30. Ash D, Sudhahar V, Youn S-W et al (2021) The P-type ATPase transporter ATP7A promotes angiogenesis by limiting autophagic degradation of VEGFR2. Nat Commun 12:3091. https://doi.org/10.1038/s41467-021-23408-1
31. Kofler N, Corti F, Rivera-Molina F et al (2018) The Rab-effector protein RABEP2 regulates endosomal trafficking to mediate vascular endothelial growth factor receptor-2 (VEGFR2)-dependent signaling. J Biol Chem 293:4805–4817. https://doi.org/10.1074/jbc.m117.812172
32. Smith GA, Fearnley GW, Abdul-Zani I et al (2016) VEGFR2 trafficking, signaling and proteolysis is regulated by the ubiquitin isopeptidase USP8. Traffic 17:53–65. https://doi.org/10.1111/tra.12341
33. Maghsoudlou A, Meyer RD, Rezazadeh K et al (2016) RNF121 inhibits angiogenic growth factor signaling by restricting cell surface expression of VEGFR-2. Traffic 17:289–300. https://doi.org/10.1111/tra.12353
34. Huckaba TM, Gennerich A, Wilhelm JE et al (2011) Kinesin-73 is a processive motor that localizes to Rab5-containing organelles. J Biol Chem 286:7457–7467. https://doi.org/10.1074/jbc.m110.167023
35. Bentley M, Decker H, Luisi J, Banker G (2015) A novel assay reveals preferential binding between Rabs, kinesins, and specific endosomal subpopulations. J Cell Biol 208:273–281. https://doi.org/10.1083/jcb.201408056
36. Delevoye C, Miserey-Lenkei S, Montagnac G et al (2014) Recycling endosome tubule morphogenesis from sorting endosomes

requires the kinesin motor KIF13A. Cell Rep 6:445–454. https://doi.org/10.1016/j.celrep.2014.01.002
37. Mills J, Hanada T, Hase Y et al (2019) LDL receptor related protein 1 requires the I3 domain of discs-large homolog 1/DLG1 for interaction with the kinesin motor protein KIF13B. Biochim Biophys Acta Bba Mol Cell Res 1866:118552. https://doi.org/10.1016/j.bbamcr.2019.118552
38. Bolis A, Coviello S, Visigalli I et al (2009) Dlg1, Sec8, and Mtmr2 regulate membrane homeostasis in Schwann cell myelination. J Neurosci 29:8858–8870. https://doi.org/10.1523/jneurosci.1423-09.2009
39. Yamada KH, Hanada T, Chishti AH (2007) The effector domain of human Dlg tumor suppressor acts as a switch that relieves autoinhibition of kinesin-3 motor GAKIN/KIF13B. Biochemistry 46:10039–10045. https://doi.org/10.1021/bi701169w
40. Hanada T, Lin L, Chandy KG et al (1997) Human homologue of the drosophila discs large tumor suppressor binds to p56 lck tyrosine kinase and shaker type Kv1.3 potassium channel in T lymphocytes*. J Biol Chem 272:26899–26904. https://doi.org/10.1074/jbc.272.43.26899
41. Kanai Y, Wang D, Hirokawa N (2014) KIF13B enhances the endocytosis of LRP1 by recruiting LRP1 to caveolae. J Cell Biol 204:395–408. https://doi.org/10.1083/jcb.201309066
42. Basagiannis D, Christoforidis S (2016) Constitutive endocytosis of VEGFR2 protects the receptor against shedding. J Biol Chem 291:16892–16903. https://doi.org/10.1074/jbc.m116.730309
43. Corti F, Ristori E, Rivera-Molina F et al (2022) Syndecan-2 selectively regulates VEGF-induced vascular permeability. Nat Cardiovasc Res 1:518–528. https://doi.org/10.1038/s44161-022-00064-2
44. Silva JAF, Qi X, Grant MB, Boulton ME (2021) Spatial and temporal VEGF receptor intracellular trafficking in microvascular and macrovascular endothelial cells. Sci Rep UK 11:17400. https://doi.org/10.1038/s41598-021-96964-7
45. Goerges AL, Nugent MA (2003) Regulation of vascular endothelial growth factor binding and activity by extracellular pH. J Biol Chem 278:19518–19525. https://doi.org/10.1074/jbc.m211208200
46. Lanahan A, Zhang X, Fantin A et al (2013) The neuropilin 1 cytoplasmic domain is required for VEGF-A-dependent arteriogenesis. Dev Cell 25:156–168. https://doi.org/10.1016/j.devcel.2013.03.019
47. Maxfield FR, McGraw TE (2004) Endocytic recycling. Nat Rev Mol Cell Bio 5:121–132. https://doi.org/10.1038/nrm1315
48. Gampel A, Moss L, Jones MC et al (2006) VEGF regulates the mobilization of VEGFR2/KDR from an intracellular endothelial storage compartment. Blood 108:2624–2631. https://doi.org/10.1182/blood-2005-12-007484
49. Wang X, Valls AF, Schermann G et al (2017) YAP/TAZ orchestrate VEGF signaling during developmental angiogenesis. Dev Cell 42:462-478.e7. https://doi.org/10.1016/j.devcel.2017.08.002
50. Hirokawa N, Noda Y, Tanaka Y, Niwa S (2009) Kinesin superfamily motor proteins and intracellular transport. Nat Rev Mol Cell Bio 10:682–696. https://doi.org/10.1038/nrm2774
51. Corti F, Simons M (2017) Modulation of VEGF receptor 2 signaling by protein phosphatases. Pharmacol Res 115:107–123. https://doi.org/10.1016/j.phrs.2016.11.022
52. Shibuya M, Claesson-Welsh L (2006) Signal transduction by VEGF receptors in regulation of angiogenesis and lymphangiogenesis. Exp Cell Res 312:549–560. https://doi.org/10.1016/j.yexcr.2005.11.012
53. Clegg LW, Gabhann FM (2015) Site-specific phosphorylation of VEGFR2 is mediated by receptor trafficking: insights from a computational model. Plos Comput Biol 11:e1004158. https://doi.org/10.1371/journal.pcbi.1004158
54. Bhattacharya R, Kwon J, Wang E et al (2008) Src homology 2 (SH2) domain containing protein tyrosine phosphatase-1 (SHP-1) dephosphorylates VEGF receptor-2 and attenuates endothelial DNA synthesis, but not migration. J Mol Signal 3:8–8. https://doi.org/10.1186/1750-2187-3-8
55. Sinha S, Vohra PK, Bhattacharya R et al (2009) Dopamine regulates phosphorylation of VEGF receptor 2 by engaging Src-homology-2-domain-containing protein tyrosine phosphatase 2. J Cell Sci 122:3385–3392. https://doi.org/10.1242/jcs.053124
56. Chittenden TW, Claes F, Lanahan AA et al (2006) Selective regulation of arterial branching morphogenesis by synectin. Dev Cell 10:783–795. https://doi.org/10.1016/j.devcel.2006.03.012